Russian Chemical Reviews **85** (3) 248 – 279 (2016) © 2016 Russian Academy of Sciences and Turpion Ltd

DOI 10.1070/RCR4547

Photocatalytic activity of layered perovskite-like oxides in practically valuable chemical reactions †

I A Rodionov, I A Zvereva

Saint Petersburg State University
Universitetskaya nab. 7 – 9, 199034 St Petersburg, Russian Federation

The photocatalytic properties of layered perovskite-like oxides corresponding to the Ruddlesen – Popper, Dion – Jacobson and Aurivillius phases are considered. Of the photocatalytic reactions, the focus is on the reactions of water splitting, hydrogen evolution from aqueous solutions of organic substances and degradation of model organic pollutants. Possibilities to conduct these reactions under UV and visible light in the presence of layered perovskite-like oxides and composite photocatalysts based on them are shown. The specific surface area, band gap energy, particle morphology, cation and anion doping and surface modification are considered as factors that affect the photocatalytic activity. Special attention is paid to the possibilities to enhance the photocatalytic activity by intercalation, ion exchange and exfoliation, which are inherent in this class of compounds. Conclusions are made about the prospects for the use of layered perovskite-like oxides in photocatalysis.
The bibliography includes 253 references.

Contents

I.	Introduction	248
II.	General notes on photocatalysis	249
III.	Layered perovskite-like oxides	252
IV.	Layered potassium hexaniobate $K_4Nb_6O_{17}$	255
V.	Ruddlesden – Popper phases	257
VI.	Dion – Jacobson phases	262
VII.	Aurivillius phases	266
VIII.	Conclusion	273

I. Introduction

The mankind is now facing new great challenges as a result of technological advances of the 20th and 21st centuries. One challenge is the threat of depletion of conventional energy sources, such as oil, gas and coal. Another one is an environmental impact caused by the use of these energy sources, namely, environmental pollution and greenhouse effect. A way to overcome these problems lies in the development of alternative (non-conventional) energy sources, development of waste-free technologies and the use of environmentally friendly fuels.[1]

Investigations into photocatalysis and design of new efficient photocatalysts can contribute to the progress in all three trends. First and foremost, solar radiation can be used for carrying out chemical reactions that would result either in energy storage or in degradation of unwanted substances.[2] One very attractive reaction in this respect is water splitting to produce hydrogen, an environmentally friendly fuel.[3,4] Of certain interest are also the reduction of carbon dioxide[5,6] and the fixation of atmospheric nitrogen.[7] These reactions use conventionally available reactants, which can be photocatalytically converted to valuable products. Further, photocatalysis has found use as a

I A Rodionov Candidate of Chemical Sciences, Senior Lecturer of the Department of Chemical Thermodynamics and Kinetics at the Institute of Chemistry, SPbSU.
Telephone: +7(812)428 – 4051, e-mail: i.rodionov@spbu.ru
Current research interests: heterogeneous photocatalysis, photocatalytic water splitting, hydrogen production, water purification, layered perovskite-like oxides, ion-exchange reactions, intercalation, exfoliation of layered oxides, composite photocatalysts.
I A Zvereva Doctor of Chemical Sciences, Professor of the same Department.
Telephone: +7(812)428 – 4051, e-mail: irina.zvereva@spbu.ru
Current research interests: inorganic materials, thermodynamics and kinetics of solid-phase processes, layered perovskite-like oxides, their structure and magnetic properties, photocatalysis, water splitting, hydrogen production, water purification.

Received 2 December 2014
Uspekhi Khimii **85** (3) 248 – 279 (2016); translated by O P Fedorova

† This review continues the series of publications on the topic 'Design and Physicochemical Characterization of New Materials' [see *Russian Chemical Reviews* **85** (1) 2016].

destructive method for removal of organic pollutants.[8–11] In particular, titania, which is the best studied and popular photocatalyst, is used in air purification devicess[12] and for creating self-cleaning coatings.[13] Development of devices for photocatalytic purification of water is also underway.[14, 15]

Search for new photocatalysts to obtain an alternative to titania is stipulated by the need to shift the performance from the UV to visible spectral range and to enhance the efficiency of photocatalysis in general. A great many inorganic compounds (oxides, nitrides or sulfides) containing almost all types of metals (alkali, alkaline earth, transition or rare earth metals) in some form have been synthesized and tested as photocatalysts in the last few decades. The diversity of existing photocatalysts was reflected in the survey articles published in recent years (see Refs. 4, 16–20).

The ability of $K_4Nb_6O_{17}$ to split water under UV light with a quantum efficiency of 3.5%, which was higher than for any of analogues existing at that time, was discovered in the late 1980s.[21] The very high activity of this niobate was interpreted as arising from its layered structure, and this stipulated large-scale studies of photocatalytic properties of other layered materials, specifically layered perovskite-like oxides.[22]

Layered perovskite-like oxides are attractive for research due to their structural specifics and some unique properties, in particular, the ability to intercalate molecules into their interlayer space, ion-exchange reactions and exfoliation to nanosheets.[23] Not only are these properties responsible for the high photocatalytic activities of some layered oxides, but they also open a way to modify them, specifically with the purpose to design composite photocatalysts and other functional materials.[24]

In this review, we analyze the photocatalytic activity in representatives of three main classes of layered perovskite-like oxides, namely Ruddlesden–Popper, Dion–Jacobson and Aurivillius phases. Although layered niobate $K_4Nb_6O_{17}$ is not a perovskite-like oxide, we found it useful to pay attention to this compound, as the methodology of photocatalytic studies of layered oxides was first worked out for it and it remains interesting up to now.[25–27]

A distinctive feature of our review consists in that we consider the photocatalytic properties of layered perovskite-like oxides in relation to their physicochemical properties, in particular, intercalation and ion-exchange properties. One major objective of the review is to use these properties to show the specifics of layered perovskite-like oxides as photocatalysts and demonstrate their potential for use in design of new photocatalytic systems. To our knowledge, no similar reviews have yet been published.

Of the photocatalytic reactions, this review focuses on water splitting and the degradation of alcohols and organic dyes in aqueous solutions for the reason that most documents on the topic deal with these reactions. We also consider other reactions that are less frequently addressed by researchers engaged in layered oxides but are of interest for application, namely, oxidation of phenols in aqueous solution, degradation of organic compounds in a gas phase and reduction of CO_2.

In order to provide the reader with a better understanding of the topics, we found it useful to start our survey with the basic data on heterogeneous photocatalysis and the structure and properties of layered perovskite-like oxides and define the terms that will be most frequently used. In Conclusion, we will submit our inferences about the advances in the field of photocatalytic properties of layered perovskite-like oxides and outline the promising lines for future research.

II. General notes on photocatalysis

II.1. General principles

Photocatalysis is the term used in reference to a change in the rate of a chemical reaction or its initiation under the action of ultraviolet, visible or IR radiation in the presence of a substance (the photocatalyst) that absorbs radiation and is involved in the chemical transformation of the reaction partners to recover its initial state after each transformation cycle.[28, 29] In accordance with this definition, the light is an inevitable partner in a photocatalytic reaction and is to be absorbed precisely by the photocatalyst.

Unlike ordinary catalysis, photocatalysis makes it possible, due to the energy of light, to implement those chemical reactions that themselves are thermodynamically unfavourable. In this case, the energy of light is partially stored in reaction products. When a dark reaction is thermodynamically allowed, the energy of light dissipates completely, and the role of light is only to facilitate the overcoming of the activation barrier by reaction partners.[30]

Homogeneous photocatalysis[31] and heterogeneous photocatalysis[32] are distinguished from each other by whether the photocatalyst and reactants are in one phase or not. In heterogeneous photocatalysis, the catalyst is, as a rule, solid while reactants are in a liquid (solution) or gaseous state. Chemical transformations occur at the interface. Semiconductor compounds are usually used as heterogeneous photocatalysts; their operation mechanism will be described below.

II.2. Mechanism of heterogeneous photocatalysis

When the absorbed quantum of light has an energy exceeding the band gap energy of a semiconductor, an electron is transferred from the valence band to the conduction band to generate a hole (vacancy) in the valence band. Electrons and holes migrate toward the photocatalyst surface and participate in redox reactions with adsorbate compounds (Fig. 1).[33]

The possibility of occurrence of a reaction is determined by the mutual positions of the reduction potentials and the band gap edges.[30] The complete photocatalytic process, which consists of at least two (oxidation and reduction) half-reactions, is possible only when both reduction potentials lie inside the band gap on the energy scale, as shown in Fig. 2 for water splitting into hydrogen and oxygen.

For water splitting to occur, the potential of the bottom of conduction band should be above zero (see Fig. 2) and the potential of the top of valence band should be below 1.23 V. This arrangement of potentials is necessary for this process from the thermodynamic standpoint, but from the kinetic standpoint, this is insufficient. The hydrogen ion reduction to generate dihydrogen is a two-electron process, and the oxidation of water to dioxygen is a four-electron process; that is, these reactions are kinetically complex and multiple-stepped. The concurrence of one-electron (primary) oxidation and reduction of water requires a potential difference of at least 5 V (see Fig. 2). For this reason,

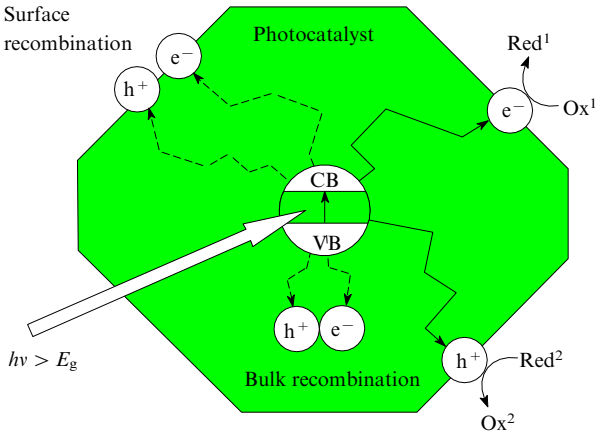


Figure 1. Heterogeneous photocatalysis scheme (adapted from Ref. 16).
VB is valence band, CB is conduction band, E_g is band gap width, $Red^{1,2}$ and $Ox^{1,2}$ are reduced and oxidized species of compound 1 and compound 2, respectively.

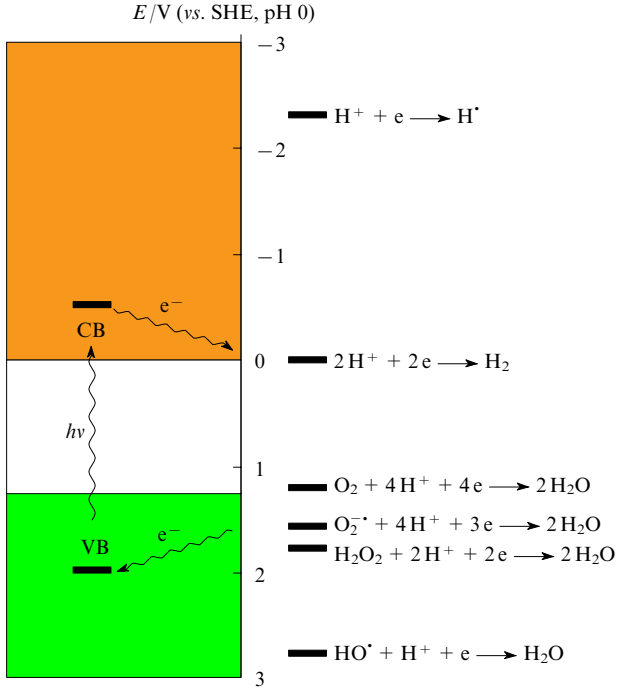


Figure 2. The energy diagram of water splitting over a semiconductor photocatalyst (reduction potentials are given according to Refs 34 and 35).
SHE is standard hydrogen electrode.

hydrogen and oxygen evolution is associated with a rather high overvoltage, which depends on the electrode material, on its ability to decrease the energy of intermediate states.[36]

Loading a cocatalyst onto the working surface of a photocatalyst is used to lower the overvoltage.[37] Platinum or nickel nanoparticles are most frequently used as cocatalysts for hydrogen evolution.[38,39] Search for suitable cocatalysts for oxygen evolution yet remains topical; RuO_2 is now used most frequently.[40]

II.3. Requirements for photocatalysts

In addition to the above-listed factors, there are some conditions the fulfillment of which is desirable to make the photocatalytic process efficient, namely:[41]

— The photocatalyst should efficiently absorb light to generate electron–hole pairs;

— The number of charge carriers that reach reaction sites (most frequently, the crystal surface) should be as great as possible; that is, the migration of electrons and holes to reaction sites should prevail over bulk electron–hole recombination; this is enhanced by a reduction in photocatalyst particle size and a reduction in defect density, or improvement of crystallinity;

— Surface recombination should be minimized; therefore, it is advisable to create conditions for the spatial separation of oxidation and reduction reaction sites;

— In order to carry out a reaction that is thermodynamically unfavourable in the absence of light, special conditions should be created for this reaction to occur irreversibly; a way to achieve this is to spatially separate the reduction and oxidation sites and to use some specific modification methods to prevent the contact between the oxidized products and reduction sites (or *vice versa*);[42]

— The photocatalyst material should be stable under reaction conditions; that is, it should not experience photocorrosion or be involved in irreversible reactions with components of the reaction medium (solution or gas).

II.4. Band gap energy

The band gap energy has a dual effect on photocatalytic activity. On the one hand, the band gap energy determines the spectrum of action of the photocatalyst: the lower the value of E_g, the longer the wavelength of the absorbable light. For the visible light to be absorbed, the prerequisite is that $E_g < 3$ eV; photocatalysts with wider band gaps are active only when exposed to UV radiation. On the other, the band gap energy and its position relative to the reduction potentials of the target half-reactions determine the reactivities of electrons and holes. Therefore, as a rule, an increase in band gap energy increases the quantum efficiency; provided that $h\nu > E_g$ and the other conditions are equal (as possible), this increase is manifested as an increased photocatalytic reaction rate.[43,44]

II.5. Specific surface area

The specific surface area is an important characteristic of a solid catalyst, and photocatalysts are no exception. Since the reaction involves the surface active sites of the catalyst, the reaction rate naturally depends on the catalyst surface area. However, the specifics of photocatalysis is that the number of active sites per unit surface area is not a fixed value, as active sites are generated by radiation (due to photoexcitation and capture of charge carriers) and are killed in the reaction.[45] The constancy of the number of active sites is a result of the acquisition of a steady state, and the specific surface area, along with some other factors, affects the steady-state number of active sites. As the specific surface area becomes larger, the number of active sites usually increases due to decreasing bulk charge carrier recombination and increasing probability of the capture of

charge carriers by the surface.[46] As a result, the photocatalytic activity is frequently in direct proportion to the specific surface area,[47,48] and methods for producing photocatalysts having developed surfaces are a popular field of research.[49,50]

II.6. Photocatalytic activity

Strictly speaking, photocatalytic activity is determined as the number of reaction product species formed as a result of the photocatalytic process divided by the number of light quanta absorbed by the photocatalyst at the given wavelength or in the given spectral range. In the former, the photocatalytic activity is referred to as the quantum yield, and in the latter, as the quantum efficiency of the reaction.[28] Thus, the photocatalytic activity is not a universal characteristic of a compound; rather, it can be determined only for a specific reaction and only for specific conditions (radiation wavelength, composition of the reaction mixture, temperature and pressure).

In experimental studies, however, the photocatalytic activity of the sample is most frequently understood merely as the rate of the chemical reaction under study, regardless of the number of absorbed photons (in view of the difficulty of its determination).[51] If so, the photocatalytic activity becomes dependent on an even greater number of experimental factors, such as the catalyst amount, radiation source power, and photoreactor design. With this approach, a correct comparison between samples can involve only photocatalytic activity values obtained under absolutely identical experimental conditions and on the same setup.[52]

In view of the foregoing, in this review we cite numerical values of photocatalytic activities (more strictly, reaction rates) only when their correct comparison can be made. Otherwise, we confine ourselves to qualitative analysis. Quantum efficiency values are given for those few systems for which they have been determined.

II.7. Types of photocatalytic reactions

The above-considered mechanism of heterogeneous photocatalysis, in general, suggests no selectivity toward any specific type of redox process. Therefore, photocatalysis makes it possible to carry out a wide spectrum of chemical reactions including conversions of both organic compounds (oxidation, reduction, substitution, isomerization, condensation, polymerization, *etc.*)[53–55] and inorganic compounds (redox reactions in solution and electrodeposition of metals).[9,56]

From a practical point of view, photocatalysis is considered as a method for the degradation of hazardous substances (water and air decontamination),[57] fuel production (water splitting and carbon dioxide reduction)[58] and organic synthesis.[59] Most studies of the photocatalytic properties of layered perovskite-like oxides concern three types of reactions: water splitting, hydrogen production from an aqueous solution of a sacrificial agent and degradation of organic dyes. We will briefly dwell on the specifics of these processes.

Water splitting. In the context, this is a process where stoichiometric amounts of hydrogen and oxygen are simultaneously evolved without consumption of any material but water. The reaction solution can comprise compounds that remain unaltered in the course of the photocatalytic reaction but generate necessary conditions (*e.g.*, KOH generates an alkaline medium).

The discovery of the very feasibility of light-driven water splitting[60] at that time was (and still is) a powerful incentive for research in the field of photocatalysis. Classic photocatalysts (TiO_2 and $SrTiO_3$) fail to provide high efficiency in water splitting, and layered oxides appeared to be a class of photocatalysts that made it possible to advance in this direction far forward.[61]

Hydrogen production from aqueous solutions of sacrificial agents. The water splitting reaction has a great positive value of Gibbs energy change ($\Delta G^\circ = 237$ kJ mol^{-1}) and comprises two half-reactions, each having kinetic hindrances.[16] An appreciable increase in overall rate can be achieved by replacing one of the two half-reactions by another one that is more easily implementable.[62] When, for example, silver nitrate is added to the reaction solution, proton reduction to hydrogen is replaced by a more preferable process where Ag^+ cations are reduced to metallic silver, to increase oxygen evolution rates.[63] In the same manner, when reducing agents are added, hydrogen evolution rates increase due to the replacement of the water oxidation half-reaction by a more preferable reaction.[64] The most frequently used reducing agents are methanol and other alcohols, and inorganic ions: I^-, Br^-, CN^-, S^{2-}, SO_3^{2-}, Fe^{2+} and Ce^{3+} (see Ref. 16). Such the additives are referred to as sacrificial agents, as they are consumed in the course of the photocatalytic reaction. Water splitting will be an incorrect name for the process by which hydrogen is released from an aqueous solution of a sacrificial agent.

Reasons for the use of sacrificial agents in photocatalytic studies can be the following:

— comparison of hydrogen evolution rates over photocatalysts that are incapable of splitting pure water, in order to establish fundamental correlations between the photocatalytic activity and structure (composition) of the sample;[65]

— with the view for practical application in case where the sacrificial agent is a material that needs recycling;[66,67]

— in two-photon photocatalytic water splitting systems, where the sacrificial agent is consumed in one portion of the system and is regenerated in another (Z scheme).[68,69]

The use of sacrificial agents in photocatalysis can cause adverse and unobvious effects that would appreciably hamper the interpretation of experimental data. For example, Ag^+ cations are reduced to be deposited on the photocatalyst surface as silver nanoparticles, which can greatly influence both optical and catalytic properties of the material.[70]

When sacrificial agents are alcohols, a current-doubling effect can appear important. This effect can be described as follows: a radical generated upon the primary oxidation of the alcohol by a photogenerated hole can appear a sufficiently strong reductant to transfer an electron to the conduction band of the photocatalyst. Hence, a doubled amount of hydrogen can be released per photogenerated electron–hole pair compared to the expectations.[70]

Importantly, the ability of the photocatalyst to release hydrogen from water in the presence of sacrificial electron donors and to release oxygen in the presence of sacrificial electron acceptors does not ensure that these products would be generated simultaneously upon splitting of pure water. Thus, while the use of sacrificial agents in photocatalysis is sometimes quite substantiated, the interpretation of results will need some caution.

Degradation of organic dyes. The choice of organic dyes (such as Methylene Blue, Methyl Orange, and Rhodamine B) as model water contaminants is guided by both the challenging environmental pollution by these compounds [71] and the ease of experimentation as they can be determined spectrophotometrically, specifically *in situ*.[72] However, this choice has some essential disadvantages.

On the one hand, the discoloration of solution can only signify the degradation of initial dye molecules and not their complete mineralization. The photocatalytic degradation of organic dyes has a complex and multistep scheme;[73] it can appear that intermediate products exceed the initial compounds in toxicity, and this casts doubt on the applicability of the process. In view of this, not only the starting materials should be analyzed. Intermediates should also be detected, although this is far more difficult and is usually not performed.

There are two major schemes for the photocatalytic degradation of organic compounds in aqueous solution: direct oxidation and indirect oxidation. In the former case, an adsorbed substrate reacts directly with a surface oxidation site of the photocatalyst; in the latter case, it is oxidized by reactive species that are generated by the oxidation of water or the reduction of dioxygen (*e.g.*, $HO^{\bullet}$).[74]

Another possible degradation scheme for organic dyes is when the light is absorbed not by the solid catalyst but rather by the dye itself.[75] This process is not photocatalytic and bears no information about the photocatalytic activity of the sample; with another dye, the reaction scheme will be completely different. Thus, dyes are far from being very suitable model substrates for assessing photocatalytic activities.[76] A researcher working with dyes should necessarily keep in mind that the reaction can follow the above-described scheme, especially when the visible light is used for irradiation.

III. Layered perovskite-like oxides

III.1. Structure and classification

Layered perovskite-like oxides are crystalline compounds where two-dimensional perovskite blocks (sheets) alternate in a regular manner with sheets of another structure. This is not a mere geometric alternation, but rather the intergrowth of layers of differing structure types.

The perovskite structure ($CaTiO_3$; general notation: ABO_3) can conveniently be imaged as corner-sharing octahedra. Every octahedron is centred by a compact cation B; the corners are occupied by oxygen atoms. Larger cations A are positioned in between octahedra in 12-coordinate oxygen surrounding. Perovskite layers in layered perovskite-like oxides can have various values of thickness (n), which is determined by the number of oxygen octahedra positioned between two neighbouring sheets of different structures. Accordingly, mono-layered, double-layered, triple-layered, *etc*. perovskite-like oxides are distinguished, where the value of $n = \infty$ corresponds to the ordinary perovskite structure (Fig. 3).[77]

The region between perovskite layers, which is populated by cations or cation–anion moieties where another structure type exists, are frequently referred to as the interlayer space. Three major classes of layered perovskite-like oxides are distinguished depending on the structure of interlayer space: Ruddlesden–Popper phases, Dion–Jacobson phases and Aurivillius phases (Fig. 4).

Compounds that form Ruddlesden–Popper phases can be represented by the general formula $A_{n+1}B_nO_{3n+1}$ (see Refs 78 and 79). They typically have an alternation of perovskite sheets (n octahedra thick) with sheets having NaCl structure. The value $n = 1$ corresponds to K_2NiF_4 type structure; $n = 2$ corresponds to $Sr_3Ti_2O_7$ type structure. An important feature of Ruddlesden–Popper phases

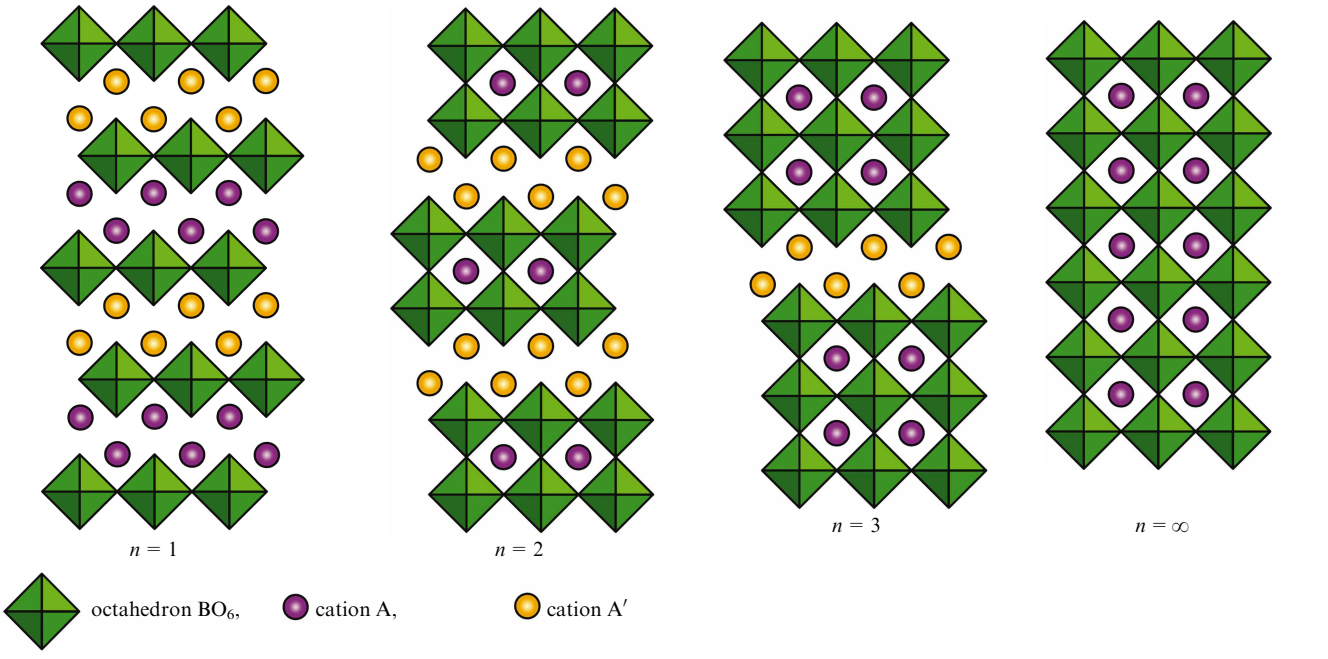


Figure 3. Layered perovskite-like oxides having various perovskite sheet thicknesses n (adapted from Ref. 77).

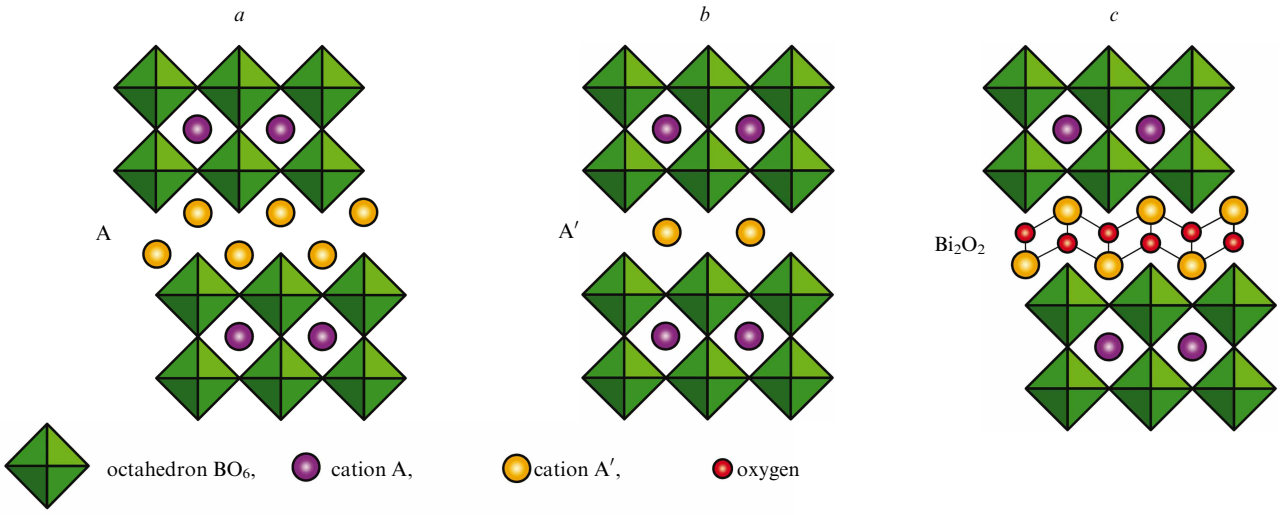


Figure 4. Structures of layered perovskite-like oxides that belong to different classes (adapted from Ref. 23). Phase notations: (*a*) Ruddlesden–Popper, (*b*) Dion–Jacobson and (*c*) Aurivillius phases.

where $n = 1$ is the nonexistence of a 12-coordinate position typical of perovskite structure: cations A reside in nine-coordinate positions.

Dion–Jacobson phases were first synthesized by Dion,[80], and then extensively studied under the supervision of Jacobson.[81, 82] The general formula of these compounds can be written as $A'[A_{n-1}B_nO_{3n+1}]$ (where A′ stands for an alkali metal, A for an alkaline earth or rare earth metal and B for a pentavalent metal, most frequently, tantalum or niobium). Perovskite layers in these compounds are interleaved with layers that comprise only metal cations, which are eight-coordinate.

Aurivillius phases, which have the general formula $A_{n-1}Bi_2B_nO_{3n+3}$, were first described in 1949.[83] Their crystal structures are formed by an alternation of *n* perovskite layers and fluorite layers, which consist of bismuth and oxygen atoms. For this reason, the composition and structure of an Aurivillius phase are described by the general formula $(Bi_2O_2)A_{n-1}B_nO_{3n+1}$; most recent studies use just this formula. Apart from the photocatalytic activity, ferroelectric properties of Aurivillius phases are also attractive to researchers.[84]

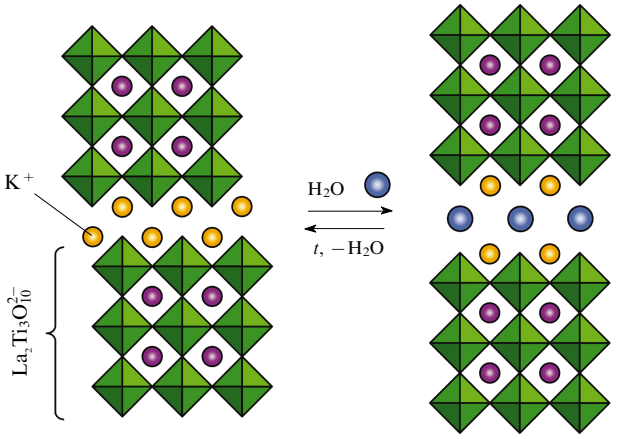


Figure 5. Scheme of water intercalation into the interlayer space of a layered oxide exemplified by $K_2La_2Ti_3O_{10}$ (adapted from Ref. 85).

III.2. Intercalation

In the context of layered oxides and related compounds, intercalation is to be understood as the reversible reaction of incorporation of some species into the interlayer space. The structural integrity of the layered oxide is preserved upon intercalation; only linear dimensions of a crystal increase in the direction normal to the plane of layers (Fig. 5).[85]

The ability of a layered oxide to be intercalated with some compound is hardly predictable beforehand, as it is determined by a set of structural and energy factors and by external settings.[86] For these reasons, intercalation of layered oxides is studied experimentally, primarily based on the determination of unit cell parameters by X-ray diffraction.[87] Useful information on intercalation/deintercalation can be gained from thermal analysis (thermogravimetry and differential scanning calorimetry)[88] and from IR spectroscopy.[89]

The ability of layered oxides to be intercalated with water attracted the attention of researchers engaged in the photocatalytic activity of layered oxides, as water splitting to hydrogen and oxygen is the primary task of such research. Water consists of small polar molecules, which are capable of hydrogen bonding (in particular, to oxygen atoms in the oxide structure), so water can easily intercalate into many layered compounds. Since some layered oxides show higher photocatalytic activities in water splitting compared to bulk oxides, it was hypothesized that water could be split not only on the surface of a layered oxide, but also in the interlayer space.[65, 90, 91] This hypothesis gives rise to some questions about the reaction scheme, primarily of how dihydrogen or dioxygen would diffuse within the

interlayer space. To our knowledge, no exhaustive answer has been found to this question. Moreover, there is no piece of strict evidence that photocatalytic water splitting can indeed occur in the interlayer space. There are only some pieces of circumstantial evidence in favour of this hypothesis (see below).

Apart from water, alcohols and organic bases also experience reversible intercalation into the interlayer space of layered oxides. Such reactions hold an important place in the chemistry of layered oxides and are significant for carrying out photocatalytic processes in the presence of these compounds.[65]

III.3. Ion-exchange reactions

Soft chemistry methods (primarily, this implies moderate reaction temperatures) are of great importance for preparing and modifying layered perovskite-like oxides.[92] Perovskite sheets, with their dominantly covalent metal–oxygen bonding, are sufficiently stable under these conditions and function as a framework in the layered oxide structure. The cations, which are mainly bonded by ionic bonds to perovskite layers in the interlayer space, are more mobile. In some cases, this makes it possible to replace some interlayer cations by other while the main structure of the layered oxide remains intact; the replacing species can be cations of another size or charge, or complex cationic species.[23] These ion-exchange reactions are carried out in solutions or in melts of appropriate salts. Of special importance is the replacement of interlayer cations by protons (protonation), which as a rule occurs in acidic aqueous solution (Fig. 6).

Ion-exchange reactions open many opportunities to the design of layered-oxide photocatalysts. These reactions can help synthesize compounds that cannot be prepared by ordinary solid-phase synthesis because of their thermal instability.[93] Ion-exchange processes enable the accommodation of cationic species in the interlayer space that would provide absorption of visible light[94] or would serve as precursors for nanoparticles to form inside the interlayer space upon subsequent treatment.[27,90] Protonated species of layered oxides are capable of intercalating organic bases due to acid–base interactions. This opens a way to further modifying these oxides by intercalation or exfoliation.

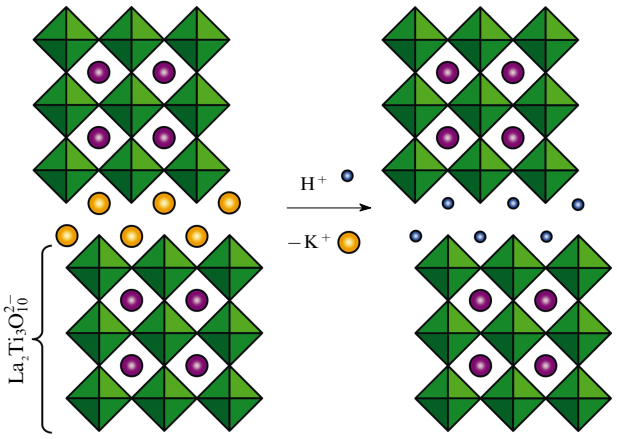


Figure 6. Protonation scheme of a layered oxide exemplified by $K_2La_2Ti_3O_{10}$ (adapted from Ref. 85).

III.4. Exfoliation of layered oxides

Liquid-phase exfoliation of layered materials has recently become popular as a method for the production of nanosized items.[95] The exfoliation of layered perovskite-like oxides to two-dimensional perovskite sheets can occur, for example, upon intercalation of bulky organic cations (such as tetra-n-butylammonium) in an appropriate solvent (Fig. 7).[96] A suspension of perovskite nanosheets is thus formed; morphologically these can be planar sheets or they can roll into tubules or scrolls.[24] When conditions (*e.g.*, pH or ionic strength) change, these nanosheets coagulate to

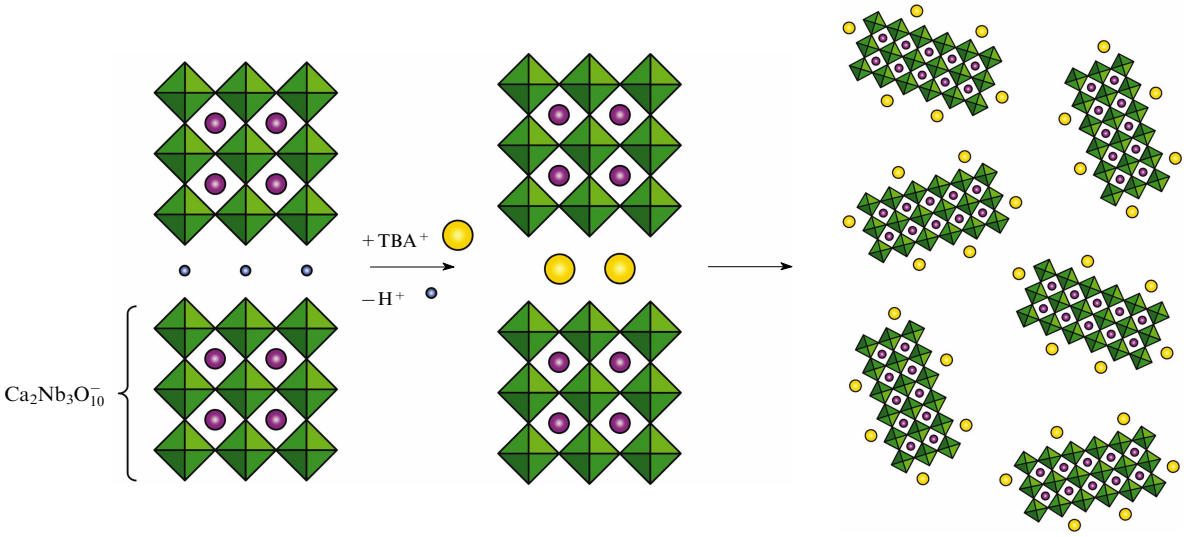


Figure 7. Exfoliation scheme of a layered oxide as a result of intercalation with tetrabutylammonium exemplified by $HCa_2Ta_3O_{10}$ (adapted from Ref. 23).

form a structure that is similar to the initial layered oxide but is most frequently disordered, porous and thereby has a developed surface.[97,98] This process is called the restacking of a layered oxide. Perovskite monolayers can intentionally be deposited from suspension to a solid substrate, which is promising for manufacturing functional coatings.[99–101]

The foregoing is obviously of importance for photocatalysis. On the one hand, the exfoliation of layered oxides followed by restacking makes it possible to enhance the photocatalytic activity through increasing specific surface area. On the other, this offers many opportunities for design of composite photocatalysts, where other entities are enclosed between perovskite monolayers and play the role of either a cocatalyst or a photosensitizer. Examples of such systems will be considered below.

IV. Layered potassium hexaniobate $K_4Nb_6O_{17}$

IV.1. Structure and principal properties

The advantage of layered-type structures over bulk structures (as in TiO_2 and $SrTiO_3$) in UV-driven photocatalytic water splitting was first shown for potassium hexaniobate $K_4Nb_6O_{17}$.[102] In 1969, Nassau *et al.*[103] prepared $K_4Nb_6O_{17}$ single crystals and addressed some properties of this compound, specifically its ability to be hydrated depending on relative humidity to form two species, namely $K_4Nb_6O_{17}\cdot 3\,H_2O$ or $K_4Nb_6O_{17}\cdot 4.5\,H_2O$. A similar compound containing rubidium instead of potassium ions, was prepared and characterized in 1980;[104] the hydration of a series of $A_4Nb_6O_{17}$ (A = K, Rb or Cs) compounds was described in detail later.[105]

The layered oxide $K_4Nb_6O_{17}$ is not a perovskite-like compound, but has much in common with these compounds in its structure and properties. The $K_4Nb_6O_{17}$ orthorhombic structure is built by niobium–oxygen octahedral layers, which alternate with potassium atoms (Fig. 8). A characteristic feature of this structure is the presence of two types of interlayer spaces, denoted as interlayer *I* and interlayer *II*. Water molecules are intercalated into interlayer *I* even when $K_4Nb_6O_{17}$ is in contact with a moist atmosphere, whereas interlayer *II* are not prone to hydration under ambient conditions.

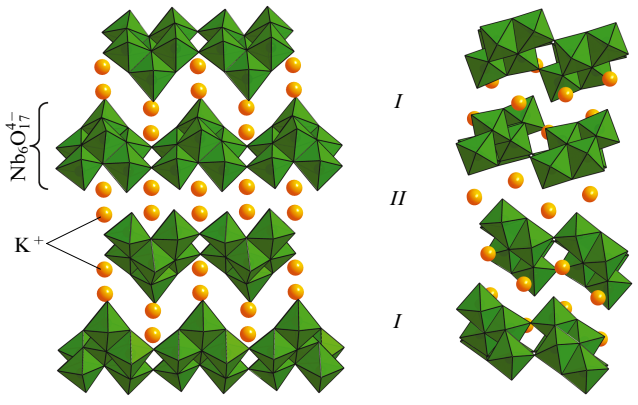


Figure 8. Structure of the layered oxide $K_4Nb_6O_{17}$.[105] *I* and *II* are different types of interlayers.

Kinomura *et al.*[106] showed that $K_4Nb_6O_{17}$ exhibits ion-exchange properties: potassium cations can be replaced by Li^+, Na^+, Ca^{2+} and Ni^{2+} cations in solutions of chlorides of these metals. The doubly charged Ca^{2+} and Ni^{2+} cations replace potassium ions only in interlayers *I*; replacement by singly charged Li^+ and Na^+ cations occurs in both types of interlayer spaces. Potassium ion replacement in interlayers *II* gives rise to its ability to be hydrated.

IV.2. Photocatalytic activity.

Effect of layered structure

The photocatalytic activity of $K_4Nb_6O_{17}$ was first documented in 1986.[102] Potassium hexaniobate manifested an extraordinary high activity in hydrogen evolution from aqueous methanol compared to the state-of-the-art photocatalysts ($SrTiO_3$ and TiO_2). When $K_4Nb_6O_{17}$ was irradiated in pure water, hydrogen was also evolved but oxygen evolution was not observed. It became possible to split water to yield stoichiometric amounts of hydrogen and oxygen only after the sample was modified with nickel by impregnation with $Ni(NO_3)_2$ solution followed by thermal decomposition of the nitrate to oxide and reduction in flowing hydrogen.

Kudo *et al.*[21] studied the influence of other modifiers, along with nickel, on the photocatalytic activity of $K_4Nb_6O_{17}$. They studied the effects of the modifier amount, modifier reduction temperature and solution pH in the course of photocatalytic reaction. Nickel was the only modifier that enhanced the photocatalytic activity of the initial sample (the optimal nickel content was 0.1 mass %). The highest quantum efficiency of water splitting, equal to $3.5\pm0.5\%$ at a wavelength of 330 nm, was achieved when the sample was subjected to reductive treatment at 400–500 °C.

Nickel-loaded $K_4Nb_6O_{17}$ was also found to withstand fairly well sulfuric acid (0.5 mol litre^{-1}), whereas in modified $SrTiO_3$, deposited nickel species dissolved completely in acid in 24 h. This implies that nickel species do not reside on the oxide surface as in the case of $SrTiO_3$ but rather occur in between niobate layers to protect them from acid.

Later research showed that the treatment of $K_4Nb_6O_{17}$ with nickel nitrate solution gives rise to a partial replacement of interlayer potassium cations by nickel cations, and reductive treatment generates very fine (~ 5 Å) nickel entities in the interlayer space, these entities playing an important role in the photocatalytic process. Kudo *et al.*[90] proved this inference by X-ray photoelectron spectroscopy, EXAFS, transmission electron microscopy and X-ray powder diffraction studies. In those studies the authors proposed a mechanism of photocatalytic water splitting over $K_4Nb_6O_{17}$ to explain its high activity. In this scheme, hydrogen evolution occurs on loaded nickel species in interlayer *I*, whereas oxygen evolution is inside interlayer *II*. Thus, the advantage of $K_4Nb_6O_{17}$ over other photocatalysts consists in that the oxidation and reduction sites lie close to each other (charge carriers have to overcome a shorter path to reach the reaction site), but are separated from each other by a niobate layer, which keeps reaction products from mixing and thereby prevents the reverse process. One piece of evidence for this is that hydrogen evolution rate over $K_4Nb_6O_{17}$ is almost independent of the presence of oxygen in the system, while this is far from being the case for other photocatalysts like $SrTiO_3$ and TiO_2.

Sayama *et al.*[107] showed that the replacement of potassium by rubidium ions provides $Rb_4Nb_6O_{17}$, which is an even more efficient photocatalyst, providing water splitting quantum efficiency of 10% at 330 nm, but the activity decreases with time. The optimal nickel content of the sample was the same as for $K_4Nb_6O_{17}$, namely 0.1 mass %.

Platinum entities, like nickel entities, increase the photocatalytic activity of $K_4Nb_6O_{17}$ by one order of magnitude when incorporated into the interlayer space of the layered oxide in the form of $[Pt(NH_3)_4]^{2+}$ cations and then reduced by hydrogen. A weakness of this method consists in that platinum entities are formed not only in the interlayer space but also on the surface of the layered oxide, which is undesirable because of their ability to catalyze the reverse water synthesis reaction.[108] Platinum entities were removed from the surface of $K_4Nb_6O_{17}$ samples by aqua regia. This approach succeeded in a partial suppression of the reverse reaction between hydrogen and oxygen. The quantum efficiency of water splitting was 1.3%.

Another efficient approach to inhibit the reverse reaction and increase the $K_4Nb_6O_{17}$/Pt photocatalytic activity was to add alkali metal carbonates to the reaction slurry.[109] The data shown in Table 1 imply that the effect of carbonates is not reduced to a mere change in pH, as the addition of alkalis does not accelerate the reaction.

The observed effect can be interpreted as follows: carbonate anions are involved in an intermediate reaction with photogenerated holes to catalyze oxygen evolution and inhibit the reverse reaction due to adsorption on platinum particles.[110] The best results in the context of water splitting rate were shown by composites prepared by platinum photoreduction. The observation that the accelerating effect of Na_2CO_3 is twice greater than that of K_2CO_3 remains unexplained.

Table 1. Effect of the composition of reaction solution on hydrogen and oxygen evolution rates over $K_4Nb_6O_{17}$/Pt (0.3%) under UV irradiation.[109]

Platinum reduction from $[Pt(NH_3)_4]^{2+}$ cation	Reaction solution		Gas evolution rate /μmol h^{-1}	
	composition	concentration /mol $litre^{-1}$	H_2	O_2
Photoreduction	H_2O		1	0
	NaOH	1.1	2	0
	KOH	1.1	1	0
	Na_2SO_4	1.1	1	0
	Na_3PO_4	0.1	2	0
	Na_2HPO_4	0.5		
	Na_2CO_3	0.3	20	7
	Na_2CO_3	1.1	124	60
	Na_2CO_3	2.2	451	217
	K_2CO_3	2.2	274	130
Reduction by hydrogen				
300 °C	Na_2CO_3	2.2	293	123
500 °C	Na_2CO_3	2.2	230	110
300 °C + aqua regia treatment	H_2O		31	13
	Na_2CO_3	2.2	214	101

Note. Parameters of the experiment: 1 g of the catalyst per 350 ml of the solution, a high-pressure mercury lamp (400 W), an internal radiation unit, a closed gas circulation system, argon pressure: 35 mm Hg.

IV.3. Photocatalysts produced by ion exchange in $K_4Nb_6O_{17}$

Ion exchange of potassium ions in $K_4Nb_6O_{17}$ for protons appreciably affects the photocatalytic activity of the niobate. Domen *et al.*[111] illustrated this effect in the reaction of UV light-driven hydrogen evolution from aqueous methanol solution (Table 2).

When a half of potassium ions in the niobate were replaced by protons in a H_2SO_4 solution, the hydrogen evolution rate increased eightfold and the quantum efficiency of the process was 30% (for $\lambda = 330$ nm); the layered oxide was not loaded with nickel. A partial exchange of potassium ions for doubly charged cations (Co^{2+}, Ni^{2+} or Cu^{2+}) leads to an almost complete inhibition of activity. The enhanced activity observed when potassium was replaced by Cr^{3+} and Fe^{3+} was ascribed to the parallel substitution of these cations for H^+ in nitrate solutions. Calcination at 500 °C, with the attendant decomposition of the hydrogen-substituted phase, deprived these samples of photocatalytic activity.

Table 2. Effect of potassium ion substitution on the photocatalytic activity of $K_4Nb_6O_{17}$.[111]

Substituent cation	Degree of substitution (%)	Hydrogen evolution rate /μmol h^{-1}
–	0	30
H^+	51	251
Cr^{3+}	66	101
Fe^{3+}	70	109
Co^{2+}	40	0
Ni^{2+}	23	3
Cu^{2+}	60	0

Note. Parameters of the experiment: 0.5 g of the catalyst per 250 ml of aqueous methanol (20 vol.%), a xenon lamp (500 W), a closed gas circulation system, argon pressure: 100 mm Hg.

IV.4. $K_4Nb_6O_{17}$/CdS composite photocatalyst

Although, in our opinion, the ion-exchange properties of $K_4Nb_6O_{17}$ *per se* and their influence on photocatalytic activity have been studied insufficiently, they are used to produce composite photocatalysts *via* incorporating various cations into the interlayer space. An example can be the synthesis of a composite where CdS particles were incorporated into $K_4Nb_6O_{17}$ through the consecutive replacement of interlayer cations by the scheme

$$K^+ \longrightarrow H^+ \longrightarrow Bu^nNH_3^+ \longrightarrow Cd^{2+}$$

followed by treatment with H_2S gas.[27]

The photocatalytic activity of the composite was studied in relation to hydrogen evolution from an aqueous solution that contained Na_2S, Na_2SO_3 and KOH. The composite under UV light had the activity three times that of the initial $K_4Nb_6O_{17}$. Under the visible light, the initial $K_4Nb_6O_{17}$ did not show photocatalytic activity, just as expected, whereas the composite sample had an activity ten times the activity

of cadmium sulfide. A likely reason behind the enhanced activity is the separation of oxidation and reduction sites due to the transition of photogenerated electrons from cadmium sulfide to the layered oxide; this transition was possible due to the mutual arrangement of the band gap bottom levels in these semiconductors. The hydrogen evolution rate was not reduced during the entire experiment (15 h); this signifies the stability of the $K_4Nb_6O_{17}$/CdS composite system, likely due to the incorporation of CdS particles in between niobate layers.

IV.5. Effect of exfoliation on the photocatalytic properties of $K_4Nb_6O_{17}$

Investigations of layered $K_4Nb_6O_{17}$ oxide in the context of its ability to exfoliate started back in the 1990s.[100] Domen *et al.*[112] exfoliated $H_4Nb_6O_{17}$ in tetra-n-butylammonium hydroxide solution, followed by restaking, to study the photocatalytic properties of the resultant material in hydrogen evolution from some alcohol solutions (Table 3).

The $H_4Nb_6O_{17}$ specific surface area increased from 4 $m^2\ g^{-1}$ in the initial compound to 108 $m^2\ g^{-1}$ in the restaked sample, but this enhanced the activity not in all cases. The initial sample had a prominent methanol decomposition selectivity compared to the restaked sample. A likely interpretation of this is that methanol molecules, which are very compact compared to other alcohol molecules, can intercalate into the interlayer space of the layered oxide and be oxidized there. These processes are less likely for ethanol and propanol. For restaked $H_4Nb_6O_{17}$, however, the hydrogen evolution rate is far less dependent on the alcohol, and in propanol decomposition, it is 18 times higher than for the initial sample (in the presence of platinum as a cocatalyst). Domen *et al.*[112] did not interpret the lower activity of platinum-loaded $H_4Nb_6O_{17}$ compared with the initial sample that they observed using ethanol and propanol. Likely, this lowering arises from the photoreduction of $PtCl_6^{2-}$complex species, which enables platinum particles to deposit only on the oxide surface. When $H_4Nb_6O_{17}$ specific surface area is low, the 1 mass % platinum content is likely to exceed the optimal value, which is manifested as surface overcoverage and a reduced light absorption efficiency. This is especially prominent for ethanol and propanol, where the reaction occurs preferably on the surface. The ratio of the platinum amount to the specific surface area is smaller in restaked $H_4Nb_6O_{17}$, so the photocatalytic activity is higher.

Table 3. Photocatalytic activity of the intact $H_4Nb_6O_{17}$ sample and an exfoliated sample.[112]

Reaction solution (10 vol.%)	H_2 evolution rate /μmol h^{-1}	
	intact sample	exfoliated sample
No cocatalyst		
Methanol	2720	490
Ethanol	225	405
Propan-1-ol	110	270
Cocatalyst 1 mass % Pt (H_2PtCl_6 photoreduction in situ)		
Methanol	3800	3200
Ethanol	110	1350
Propan-1-ol	40	720

Note. Parameters of the experiment: 1 g of the catalyst per 330 ml of aqueous alcohol solution (10 vol.%), a high-pressure mercury lamp (450 W), a closed gas circulation system, argon pressure: 100 mm Hg.

The morphology of species resulting from exfoliation depends on the organic base and conditions used. Sarahan *et al.*[113] obtained niobate nanosheets and nanoscrolls from $K_4Nb_6O_{17}$ using n-propylammonium hydroxide and tetra-n-butylammonium hydroxide, respectively. Photocatalytic activity studies of such nanoparticles directly in water splitting reaction are difficult as the nanoparticles contain adsorbate organic base molecules, which are involved in the photocatalytic process as reducing agents. Under UV light, such systems feature hydrogen evolution in amounts comparable with the amount observed for the initial layered oxide both in water and in aqueous methanol.

Exfoliated $K_4Nb_6O_{17}$ particles are promising for use, in the presence of photosensitizer dyes, in design of photocatalytic systems that would operate in the visible spectral range. Maeda *et al.*[114] showed this for hydrogen evolution from an aqueous solution of ethylenediaminetetraacetic acid (as the sacrificial agent) in the presence of aggregated niobate nanoscrolls and $Ru(bpy)_3^{2+}$ dye (bpy = 4,4′-bipyridine) on exposure to the light with $\lambda > 420$ nm. The hydrogen evolution rate appeared to be 10 times as high as with unexfoliated $K_4Nb_6O_{17}$, which was due to the photocatalyst specific surface area increasing from 1 – 2 to 250 – 300 $m^2\ g^{-1}$ and the associated higher efficiency of adsorption of $Ru(bpy)_3^{2+}$complexes.

Although the photocatalytic properties of $A_4Nb_6O_{17}$ (A = H, K or Rb) layered niobates have long been studied, these compounds are still of interest for the following reason. Having a unique structure that contains two types of interlayer spaces, along with having intrinsic water splitting photocatalytic activity, these oxides serve as an ideal matrix for the design of composite photocatalysts.

V. Ruddlesden – Popper phases

V.1. Structure and principal properties

The best studied Ruddlesden – Popper photocatalysts include triple-layered titanates, specifically $K_2La_2Ti_3O_{10}$. The structure of this compound was first characterized in 1987 (Ref. 85) and refined by Toda *et al.*[115] Layered oxide $K_2La_2Ti_3O_{10}$ can intercalate water molecules into its interlayer space (Fig. 9) without being in contact with water; exposure to humid air is sufficient. Treatment by nitric acid (2 mol $litre^{-1}$) for 5 days at room temperature gives rise to the replacement of potassium interlayer ions by protons to yield $H_2La_2Ti_3O_{10}$. This compound, unlike Dion – Jacobson phases such as $HCa_2Nb_3O_{10}$, features no noticeable acidic properties.[116]

V.2. Photocatalytic activity of $A_2La_2Ti_3O_{10}$ (A = K, Rb, Cs) titanates. Effect of layered structure

The photocatalytic activity of $K_2La_2Ti_3O_{10}$ was first documented in 1997 by Takata *et al.*[117] Having a band gap energy of 3.5 eV, this titanate appeared capable of splitting water into hydrogen and oxygen under UV light. Loading with an optimal amount of nickel oxide (3 mass %) increased the photocatalytic activity fivefold. Better results were achieved in alkaline medium with KOH concentration of 0.1 mol $litre^{-1}$. The researchers suggested that the NiO

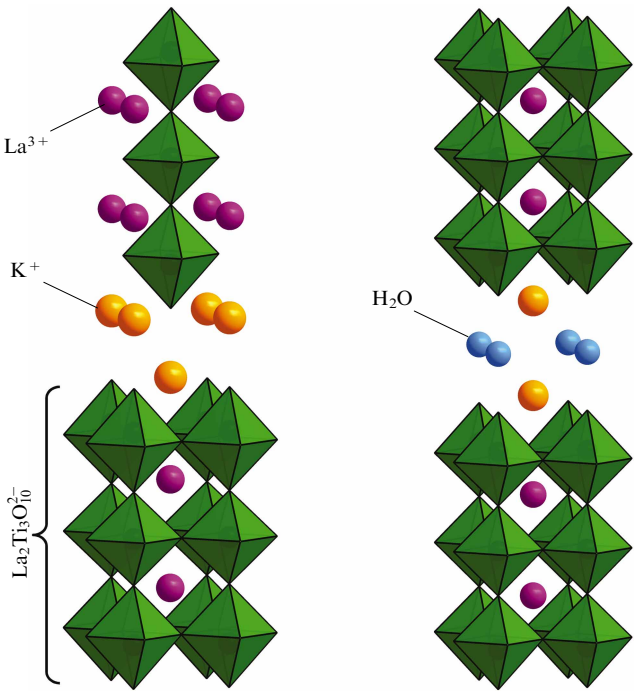


Figure 9. Structures of the layered oxide $K_2La_2Ti_3O_{10}$ and its protonated form (according to Ref. 85).

modifier species are located on the catalyst surface and serve as hydrogen evolution sites, whereas oxygen is formed due to oxidation of water in interlayers. Takata *et al.*[91] attempted to confirm this suggested mechanism for isostructural titanate $Rb_2La_2Ti_3O_{10}$,[118] which featured the activity twice as high as that of the potassium-containing analogue. A partial replacement of titanium by niobium to yield $RbLa_2Ti_2NbO_{10}$ was found to result in the complete loss of intercalation capacity due to decreasing negative charge of the perovskite layer (Table 4). In association, the photocatalytic activity decreased by an order of magnitude, in spite of the constancy of the band gap energy and particle sizes. The intermediate compound $Rb_{1.5}La_2Ti_{2.5}Nb_{0.5}O_{10}$ retains the intercalation capacity, and the photocatalytic activity remains virtually unchanged. However, it is still unclear why the contents of cocatalyst NiO_x optimal for photocatalysis change in the samples under consideration.

For $Rb_2La_2Ti_3O_{10}/NiO_x$, the quantum efficiency for photocatalytic water splitting at 330 nm was ~5%.[91] Although this layered oxide is superior to its potassium-containing analogue in photocatalytic activity, it has not been studied later as a photocatalyst, while $K_2La_2Ti_3O_{10}$ still attracts attention.

Neither $Li_2La_2Ti_3O_{10}$ nor $Na_2La_2Ti_3O_{10}$ has noticeable photocatalytic activity even in hydrogen evolution from aqueous isopropyl alcohol, probably because of lacking ability to intercalate water molecules.[64,119] As to $Cs_2La_2Ti_3O_{10}$, this compound was mentioned only once[91] as a photocatalyst the activity of which is commensurate to that of $Rb_2La_2Ti_3O_{10}$. However, the literature is completely silent about its structure and properties, maybe because of synthetic difficulties. Later photocatalytic studies of $K_2La_2Ti_3O_{10}$ followed three mainstreams, namely:

— cation/anion doping;

— photocatalytic activity as influenced by the preparation method; and

— design of composite catalysts.

V.3. Photocatalytic activity of doped $K_2La_2Ti_3O_{10}$

The most important results about the effect of doping on the $K_2La_2Ti_3O_{10}$ photocatalytic activity are shown in Table 5 together with the parameters of its synthesis and photocatalytic experiments.

The general trend is that doping of $K_2La_2Ti_3O_{10}$ in most cases increases the photocatalytic activity, at most 2–3-fold. An outstanding result (a 26-fold gain in activity) was obtained with chromium doping. Unfortunately, Yang *et al.*[121] did not show whether this effect survived when pure water was split in the absence of a sacrificial agent.

The photocatalytic activity of unmodified $K_2La_2Ti_3O_{10}$ observed in some studies under visible light might arise from one of the following factors: non-intrinsic (impurity) light absorption by the photocatalyst, light absorption by reactants (when dyes were used), and an incomplete cutoff of the UV light during experiments.

Huang *et al.*[127] attempted to dope $K_2La_2Ti_3O_{10}$ with nitrogen in order to sensitize it to visible radiation. For this purpose, the initial oxide was treated with HNO_3 (0.5 mol litre^{-1}) for 15 h, then ammonia was added and the sample was calcined at 400 °C. However, this nitric acid treatment must have resulted in complete exchange of potassium ions for protons, so it would be incorrect to speak of a sample having composition $K_2La_2Ti_3O_{10-x}N_x$, especially as heating leads to the degradation of the protonated phase.

Table 4. Photocatalytic activity and hydration of potassium- and rubidium-containing Ruddlesden–Popper phases.[91]

Sample	Optimal NiO_x content (%)	Gas evolution rate /μmol h^{-1}		Number of water molecules per formula unit
		H_2	O_2	
$K_2La_2Ti_3O_{10}/NiO_x$	3	444	221	1.0
$Rb_2La_2Ti_3O_{10}/NiO_x$	4	869	430	1.1
$Rb_{1.5}La_2Ti_{2.5}Nb_{0.5}O_{10}/NiO_x$	5	725	358	0.9
$RbLa_2Ti_2NbO_{10}/NiO_x$	0.3	79	30	0

Note. Parameters of the experiment: 1 g of the catalyst per 330 ml of 0.1 M KOH (RbOH), a high-pressure mercury lamp (450 W), an internal radiation unit, a closed gas circulation system.

Table 5. Effect of doping on the photocatalytic activity of layered oxide $K_2La_2Ti_3O_{10}$ in various model reactions.

Dopant		Synthesis method	Parameters of the experiment	Gain in activity [a]		Ref.
element	concentration (%)			UV	visible light	
			Hydrogen evolution from aqueous methanol (10 vol.%)			
Nb	3.3	Solid-phase	c_{cat} = 0.8 g litre^{-1}, Hg 450 W, λ < 400 nm	2.2	–	120
			Hydrogen evolution from KI solution			
Cr	2	Sol – gel	c_{KI} = 3.36 g litre^{-1}, pH 11.8, c_{cat} = 1.7 g litre^{-1}, Hg 250 W, 15 mW cm^{-2}, 300 < λ < 400 nm, Xe 250 W, visible light	26	5	121
B	1 – 2	The same	c_{KI} = 3.36 g litre^{-1}, pH 11.8, c_{cat} = 1.7 g litre^{-1}, Hg 250 W, 15 mW cm^{-2}, 300 < λ < 400 nm, Xe 250 W, visible light	2.7	5.2	122
B	1	"	c_{KI} = 3.36 g litre^{-1}, pH 11.8, c_{cat} = 1.7 g litre^{-1}, Hg 250 W, 15 mW cm^{-2}, 300 < λ < 400 nm, Xe 250 W, visible light	2.7	4	123
Al	1	"	c_{KI} = 3.36 g litre^{-1}, pH 11.8, c_{cat} = 1.7 g litre^{-1}, Hg 250 W, 15 mW cm^{-2}, 300 < λ < 400 nm, Xe 250 W, visible light	2.7	3.7	123
Ga	1	"	c_{KI} = 3.36 g litre^{-1}, pH 11.8, c_{cat} = 1.7 g litre^{-1}, Hg 250 W, 15 mW cm^{-2}, 300 < λ < 400 nm, Xe 250 W, visible light	2.7	3.3	123
In	1	"	c_{KI} = 3.36 g litre^{-1}, pH 11.8, c_{cat} = 1.7 g litre^{-1}, Hg 250 W, 15 mW cm^{-2}, 300 < λ < 400 nm, Xe 250 W, visible light	2.1	3	123
Zn	1.5	"	c_{KI} = 3.36 g litre^{-1}, pH 11.8, c_{cat} = 1.7 g litre^{-1}, Hg 250 W, 15 mW cm^{-2}, 300 < λ < 400 nm, Xe 250 W, visible light	2.3	3.5	124
V	1.5	"	c_{KI} = 3.36 g litre^{-1}, pH 11.8, c_{cat} = 1.7 g litre^{-1}, Hg 250 W, 15 mW cm^{-2}, 300 < λ < 400 nm, Xe 250 W, visible light	1.7	2.7	125
			Hydrogen evolution from aqueous methanol (25 vol.%)			
Fe	4	Sol – gel	c_{cat} = 0.83 g litre^{-1}, Xe 250 W, λ > 400 nm	–	2.7	126
			Hydrogen evolution from aqueous methanol (0.1 mol litre^{-1})			
N	–	Solid-phase	c_{cat} = 0.2 g litre^{-1}, Hg 300 W, λ > 290 nm	–	1.2	127
			Methyl Orange degradation (20 mg litre^{-1})			
N	–	Solid-phase	c_{cat} = 0.2 g litre^{-1}, Hg 300 W, λ > 400 nm	–	12	127
			Hydrogen evolution from aqueous methanol (10 vol.%)			
Ce	0.5	Solid-phase	c_{cat} = 5 g litre^{-1}, Xe 500 W	–	2.1	128
			Hydrogen evolution from aqueous solution of Na_2S/Na_2SO_3			
Fe	7	Solid-phase	c_{cat} = 2 g litre^{-1}, Hg 500 W, Xe 500 W	4	Activity appears	129
Ni	7		c_{cat} = 2 g litre^{-1}, Hg 500 W, Xe 500 W	–	No activity	129
W	7		c_{cat} = 2 g litre^{-1}, Hg 500 W, Xe 500 W	2	Activity appears	129
			Rhodamine B degradation (5×10^{-5} mol litre^{-1})			
Sn	–	Solid-phase	c_{cat} = 2 g litre^{-1}, Xe 450 W, 400 < λ < 800 nm	–	7	130
N	–		c_{cat} = 2 g litre^{-1}, Xe 450 W, 400 < λ < 800 nm	–	2	130

Note. Here and in the other Tables, the followiong notations are used: c_{cat} is catalyst concentration in the reaction system, Xe $n \times 100$ W and Hg $n \times 100$ W are a xenon lamp and a mercury lamp, respectively, with its wattage. [a] The factor by which the photocatalytic activity of the doped sample is greater than in an undoped sample.

V.4. Effect of the synthesis method on the photocatalytic activity of $K_2La_2Ti_3O_{10}$

Hydrothermal synthesis and sol–gel technology can yield $K_2La_2Ti_3O_{10}$ samples having surface areas larger (2–3 times) than in samples prepared by solid-phase synthesis and thereby having higher photocatalytic activities (Table 6). However, attempts to considerably increase the specific surface area of $K_2La_2Ti_3O_{10}$ by these methods failed, and therefore, there is need for new approaches to the preparation of these photocatalysts.

Zhang *et al.*[133] studied the activity of a set of $K_2Ln_2Ti_3O_{10}$ (Ln = La, Nd, Sm, Gd, Dy) samples prepared by a sol–gel method in photocatalytic Methyl Orange degradation. These samples showed a twofold to fourfold (depending on the lanthanide) increase in dye degradation rate relative to samples prepared by solid-phase synthesis. However, Rodionov *et al.*[137] showed that Methyl Orange photolysis rates (in the absence of a catalyst) depended appreciably on solution pH, which was not monitored by Zhang *et al.*[133] Thus, the observed changes in dye degradation rate could arise not so much from the change in photocatalytic activity, but rather from the ion-exchange-induced shift of pH.

V.5. $K_2La_2Ti_3O_{10}$-based composite photocatalysts

The most important results obtained through modifying $K_2La_2Ti_3O_{10}$ with metallic, oxide or sulfide species, are found in Table 7. One can see that these composites can not only possess enhanced photocatalytic activities in the UV spectral range, but they can also acquire activity in the visible range due to light absorption by modifier species. Let us dwell on some results in more detail.

An $H_2La_2Ti_3O_{10}$ composite with TiO_2 was prepared by the scheme that involved the following steps: solid-phase synthesis of $K_2La_2Ti_3O_{10}$, protonation in 2 M nitric acid, intercalation of n-hexylamine *via* treatment with its ethanolic solution (50 vol %), treatment with titanium tetraisopropoxide in hydrochloric acid (1 mol litre^{-1}) and exposure to UV light in water to degrade the intercalated amine.[141] Ultimately, the specific surface area of the resulting material was five times as large as in the initial $H_2La_2Ti_3O_{10}$, interlayers expanded and the optical absorption edge shifted from 3.4 to 3.1 eV. The rate of the model photocatalytic reaction also increased by a factor of five on the average, which correlated with the increase in specific surface area. However, since the photocatalytic activity was studied in the visible light-induced degradation of some organic dyes ($\lambda > 400$ nm), the unambiguous conclusion that the composite is superior over its constituent compounds cannot be drawn. Most likely, the light was absorbed by dyes and not by the catalyst, and the photocatalytic degradation mechanism was not operative.

A similar method was used by Wu *et al.*[142] to prepare an $H_2La_2Ti_3O_{10}$ composite with Fe_2O_3. After n-hexylamine was intercalated into the protonated form of the layered titanate, ion exchange for $[Fe_3(OAc)_7(OH)(H_2O)_2]^+$ was carried out in aqueous solution, followed by UV irradiation, to form Fe_2O_3 particles in the interlayer space. The

Table 6. Effect of the synthesis method on the photocatalytic activity of layered oxide $K_2La_2Ti_3O_{10}$.

Synthesis method	Parameters of the experiment	Gain in activity [a]		Ref.
		UV	visible light	
		Water splitting		
Sol–gel (polymeric complex)	c_{KOH} = 0.1 mol litre^{-1}, c_{cat} = 3.33 g litre^{-1}, Hg 450 W	1.7 when the surface area increases by a factor of 1.2 (explained by a decrease in number of defects)	–	131, 132
		Methyl Orange degradation (20 mg litre^{-1})		
Sol–gel (stearic acid)	c_{cat} = 1 g litre^{-1}, Hg 300 W	2; the degradation rate increases in the series La < Nd < Sm < Gd < Dy (for Dy, the gain is 4 times)	–	133
		Hydrogen evolution from KI solution		
Sol–gel under H_2 atmosphere	Hg 250 W, 15 mW cm^{-2}, 300 nm < λ < 400 nm, Xe 250 W	1.4 [b]	1.8 [b]	134
under Ar atmosphere	The same	2.2 [b]	2.4 [b]	
		Hydrogen evolution from aqueous methanol (10 vol.%)		
Hydrothermal	T = 60 °C, c_{cat} = 0.8 g litre^{-1}, Hg 450 W	2.2 due to 3.1-fold increase in surface area	–	135
		Hydrogen evolution from Na_2S–Na_2SO_3 aqueous solution		
Sol–gel (stearic acid)	c_{cat} = 4 g litre^{-1}, Hg 300 W	See [c]	–	136

[a] The factor by which the photocatalytic activity is greater than in a sample prepared by solid-phase synthesis. [b] Compared to sol–gel synthesis under air. [c] The maximal activity is observed upon calcination for 2 h at 1000 °C. No comparison with solid-phase synthesis was carried out.

Table 7. Effects of various modifiers on the photocatalytic activity of layered oxide $K_2La_2Ti_3O_{10}$.

Modifier		Parameters of the experiment	Gain in activity [a]		Ref.
oxide, element	concentration (%)		UV	visible light	
		Water splitting, c_{KOH} = 0.1 mol litre^{-1}			
NiO	3	c_{cat} = 3.125 g litre^{-1}, Hg 450 W	6	–	117
$NiO + Cr_2O_3$	3 + 0.5	c_{cat} = 3.125 g litre^{-1}, Hg 450 W, $\lambda > 190$ nm	1.7 [b]	–	138
Au	1	c_{cat} = 2.5 g litre^{-1}, 8 lamps 24 W, $\lambda = 300 \pm 50$ nm, 8 lamps 24 W, $\lambda = 419 \pm 25$ nm	–	2 [b]	139
		Hydrogen evolution from aqueous methanol (10 vol.%)			
Pt	2	c_{cat} = 5 g litre^{-1}, Hg 500 W	9	–	140
		Degradation of organic dyes (20 mg litre^{-1})			
TiO_2 (see [c])	–	c_{cat} = 0.8 g litre^{-1}, Hg 300 W, $\lambda > 400$ nm	–	5	141
		Degradation of Methyl Orange (20 mg litre^{-1})			
Fe_2O_3 (see [c])	–	c_{cat} = 0.8 g litre^{-1}, Hg 300 W, $\lambda > 400$ nm	–	17 [d]	142
CdS	–	c_{cat} = 1 g litre^{-1}, Hg 300 W, $\lambda \approx 365$ nm	1.5 [d]	–	143
		Hydrogen evolution from Na_2S–Na_2SO_3 aqueous solution			
CdS	–	c_{cat} = 2 g litre^{-1}, Hg 300 W, Xe 500 W	2	11 [d]	144 – 146
PbS	–	c_{cat} = 2 g litre^{-1}, Hg 300 W	1.5	–	147
CdS	–	c_{cat} = 5 g litre^{-1}, Xe 500 W, $\lambda > 400$ nm	–	2 [e]	148

[a] The factor by which the photocatalytic activity is greater than in a sample prepared by solid-phase synthesis. [b] Compared to a sample loaded with NiO (3%). [c] The proton-substituted form $H_2La_2Ti_3O_{10}$ was modified. [d] Compared to the modifier. [e] Compared to TiO_2, modified in the same manner.

iron percentage in the thus-prepared samples was ~8%, the optical absorption edge shifted to 2.2 eV, and the specific surface area was five times larger compared to the surface area of the initial compound. The Methyl Orange dye degradation rate under visible light ($\lambda > 400$ nm) was 40 times as high as the rate observed for $H_2La_2Ti_3O_{10}$ and 17 times as high as observed for Fe_2O_3. In this case, these observations can fairly well signify an enhanced photocatalytic activity of $H_2La_2Ti_3O_{10}/Fe_2O_3$ as this composite can absorb the visible light, unlike $H_2La_2Ti_3O_{10}/TiO_2$. The same composite was prepared by a hydrothermal method involving treatment of $H_2La_2Ti_3O_{10}$ with $Fe(NO_3)_3$ solution in an autoclave at 160 °C. The resulting composite sample had a slightly smaller specific surface area compared to the preceding sample and, accordingly, a lower photocatalytic activity.

Thaminimulla *et al.*[138] showed how the photocatalytic water splitting activity of $K_2La_2Ti_3O_{10}$ changes when the surface of a layered oxide is loaded with other metal oxides together with NiO_x (Table 8).

A positive effect was achieved only with chromium oxide; otherwise, the activity lowered. After optimizing synthesis parameters, Thaminimulla *et al.*[138] attained a photocatalytic activity for the composite $K_2La_2Ti_3O_{10}$/NiO (3%)/Cr_2O_3 (0.5%) twice as great as for the initial $K_2La_2Ti_3O_{10}$/NiO (3%). Presumably, the role of chromium oxide consists in facilitating hydrogen evolution from a Ni/NiO particle thereby to inhibit oxygen sorption.

Tai *et al.*[139] studied gold nanoparticles as an alternative to nickel oxide for use as a cocatalyst for $K_2La_2Ti_3O_{10}$. They did not achieve a higher water splitting activity under UV light; however, they managed to achieve this at $\lambda = 420$ nm, maybe because of light absorption by gold particles due to plasmon resonance.

Table 8. Effect of modifying by various oxides on the photocatalytic activity of $K_2La_2Ti_3O_{10}/NiO_x$ in water splitting reaction.[138]

Metal	Gas evolution rate /μmol h^{-1}	
	H_2	O_2
–	507	255
Cr	545	275
Mn	13	5
Fe	4	2
Co	105	0
Cu	130	4
Ru	112	1
Ag	149	74
Ce	215	104
Sm	26	3
Pb	62	0

Note. Parameters of the experiment: 1 g of the catalyst per 330 ml of 0.1 mol litre^{-1} KOH, a high-pressure mercury lamp (450 W), an internal radiation unit, a closed gas circulation system; argon pressure: 50 mm Hg.

There are only few studies concerned with the exfoliation of Ruddlesden – Popper phases of triple-layered titanates because of the difficulties to intercalate organic compounds into them. However, Schaak and Mallouk [149] showed the possibility to exfoliate $H_2La_2Ti_3O_{10}$ and

$Na_2La_2Ti_3O_{10}$ using n-butylamine and tetra-n-butylammonium hydroxide, respectively. $H_2Ln_2Ti_3O_{10}$ nanosheets were prepared by exfoliation in ethylamine solution (0.1 mol litre^{-1}) for five days in order to study their luminescent properties.[150, 151] However, the exfoliation of triple-layered titanates has not yet been used in the design of photocatalysts.

VI. Dion–Jacobson phases

VI.1. Structure and most important properties

Typical representatives of Dion–Jacobson phases are double- and triple-layered oxides $ALnB_2O_7$ and $ACa_2B_3O_{10}$, where A stands for an alkali metal, Ln for a lanthanide, and B for niobium or tantalum. These compounds have slightly differing structures depending on the alkali metal, which is manifested as a consecutive shift of neighbouring perovskite layers by 1/2 along crystallographic axes *a* and *b*, as shown in Fig. 10.[152–154]

Dion–Jacobson phases typically have ion-exchange properties. Interlayer cations can be replaced by protons upon exposure to an aqueous acid.[81, 155] Replacement of one alkali metal by another can be accomplished in the appropriate nitrate melt;[155] as a rule, a cation having a larger radius is replaced by a smaller cation. Partial replacement by doubly charged cations is also possible.[156] Due to their acidic properties, protonated compounds can react with alkalis (to exchange protons for alkali metals)[157] and intercalate a wide spectrum of organic bases, such as pyridine and n-alkylamines (having hydrocarbon chain lengths up to 18).[82, 155, 158] The intercalation of bulky organic molecules can lead to splitting of the layered structure of a Dion–Jacobson phase. In most detail this effect was studied for triple-layered niobates,[24, 46, 96, 97, 101, 112, 159–164] although other compounds can experience structure splitting, too.[150]

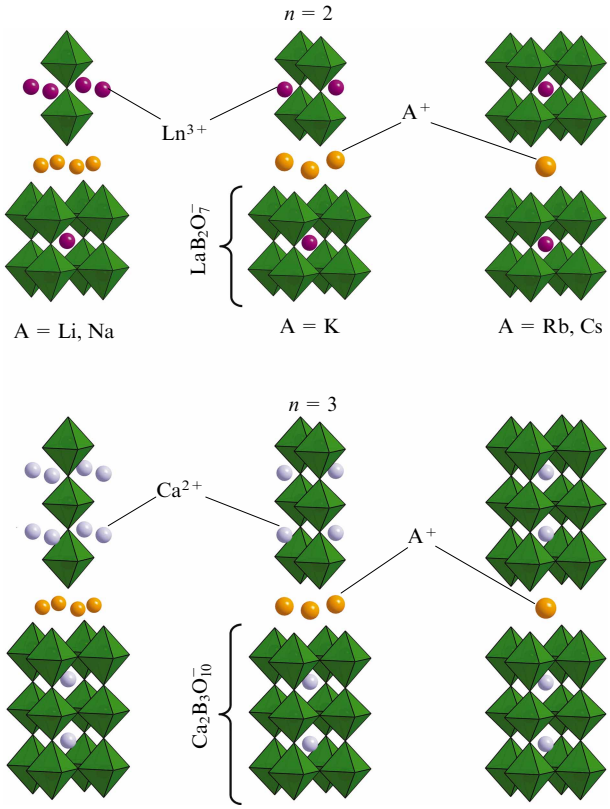


Figure 10. Structures of layered oxides $ALnB_2O_7$ and $ACa_2B_3O_{10}$.[152–154]

VI.2. Photocatalytic activity of layered niobates. Role of intercalation in photocatalysis

The activity of Dion–Jacobson phases was first studied by Domen *et al.*[65] for $ALaNb_2O_7$ and $ACa_2Nb_3O_{10}$ (A = Cs, Rb, K or H) niobates in photocatalytic hydrogen evolution and oxygen evolution from aqueous solutions of methanol and silver nitrate, respectively (Table 9). These niobates are incapable of splitting water to hydrogen and oxygen unless specially modified.[61]

Of the double-layered niobates, the rubidium-containing oxide has the highest activity (which was also confirmed by Burovikhina *et al.*[165]); of the triple-layered niobates, a potassium-containing sample has the highest activity. Platinum loading slightly increases the activity, the effect being more prominent for triple-layered oxides than for double-

Table 9. Photocatalytic activities of layered niobates in the reactions of hydrogen and oxygen evolution (μmol h^{-1}) from aqueous solutions.[65]

Sample	Number of layers	H_2 evolution				O_2 evolution	E_g/eV
		I	II	III	IV		
$K_4Nb_6O_{17}$	1	130	270	750	740	13	3.5
$KLaNb_2O_7$	2	28	54	760	3800	46	3.2
$RbLaNb_2O_7$	2	60	90	740	2600	2	3.35
$CsLaNb_2O_7$	2	12	28	300	2200	3	3.3
$KCa_2Nb_3O_{10}$	3	14	100	5900	19000	8	3.35
$RbCa_2Nb_3O_{10}$	3	3	26	3100	17000	16	3.5
$CsCa_2Nb_3O_{10}$	3	2	10	970	8300	10	3.5
$KSr_2Nb_3O_{10}$	3	10	110	8900	43000	30	3.16
TiO_2 (anatase)	–	–	7400	–	–	660	3.0

Note. Parameters of the experiment: 1 g of the catalyst, Hg 450 W, for the reaction of hydrogen evolution: 50 ml MeOH + 300 ml H_2O, for the reaction of oxygen evolution: 350 ml of a 0.01 M $AgNO_3$ aqueous solution. Notations: I and II are hydrogen evolution rates using unmodified and 0.1% Pt modified samples, respectively; III and IV are hydrogen evolution rates with unmodified and 0.1% Pt modified H^+-substituted samples, respectively.

Table 10. Photocatalytic hydrogen evolution rate as dependent on the nature of sacrificial agent for various catalysts.[65]

Alcohol	H_2 evolution rate /μmol h^{-1}			
	$KCa_2Nb_3O_{10}$	$HCa_2Nb_3O_{10}$	$HCa_2Nb_3O_{10}$/Pt (see [a])	TiO_2/Pt (see [a])
Methanol	7	920	4670	4000
Ethanol	7	73	384	5170
Propan-1-ol	3	27	43	3480
Butan-1-ol	2	19	30	2790

Note. Parameters of the experiment: 1 g of the catalyst, Hg 450 W, 50 ml alcohol + 300 ml water. [a] The catalysts are modifeid with 0.1% Pt.

Table 11. Photocatalytic hydrogen evolution rate as dependent on the nature of sacrificial agent for $HCa_2Nb_3O_{10}$ and $HCa_2Nb_3O_{10}/SiO_2$. samples.[166]

Alcohol	H_2 evolution rate /μmol h^{-1}	
	$HCa_2Nb_3O_{10}$	$HCa_2Nb_3O_{10}/SiO_2$
Methanol	4670	8100
Ethanol	347	5500
Propan-1-ol	43	1100
Butan-1-ol	60	1060

Note. Parameters of the experiment: 1 g of the 0.1% Pt-modified catalyst; Hg 450 W; 50 ml alcohol + 300 ml water.

layered oxides. A strong gain in hydrogen evolution rate is observed after interlayer cations are replaced by protons. The authors explained this by the capability of the protonated phase to intercalate water and methanol molecules into the interlayer space, where the oxidation reaction occurs. A piece of support to this hypothesis comes from the strong dependence of the hydrogen evolution rate on the nature of the sacrificial agent used (Table 10). The intercalation of an alcohol into the interlayer space becomes more difficult as the hydrocarbon chain length increases, and the photocatalytic activity weakens as a result. When the catalyst was titania (which is incapable of being intercalated), the decay in activity was not so prominent.

A similar trend can be traced for a $HCa_2Nb_3O_{10}/SiO_2$ composite sample that was prepared by intercalation of n-octylamine in heptane followed by incorporation of $Si(OEt)_4$ and thermolysis (Table 11).

After SiO_2 was loaded, the specific surface area of the sample increased from 2 to 200 $m^2\ g^{-1}$ as a result of the formation of a microporous structure in between perovskite layers, and this was expected to enhance the photocatalytic activity. However, the enhancement was distinct only in alcohols heavier than methanol. This observation provides a piece of evidence that the observed methanol degradation selectivity of the precursor $HCa_2Nb_3O_{10}$ was due to kinetic hindrances to the intercalation of larger alcohol molecules into the interlayer space. The hydrogen evolution rate over $HCa_2Nb_3O_{10}$ decreased almost by a factor of 100 from methanol to propanol, whereas the sample where the interlayer space was expanded by silica experienced only an eightfold loss of activity. Thus, when the interlayer space in the layered oxide structure is accessible to reactant molecules, it can be regarded as the working surface of the catalyst.

The dependence of hydrogen evolution rate on the degree of H^+ for K^+ cation substitution in $KCa_2Nb_3O_{10}$ also proves that a photocatalytic process occurs in the interlayer space: a strong increase in catalytic activity is observed for degrees of substitution of 70%–80%, that is, just when there appears the capability to incorporate water and methanol molecules into the interlayer space.[65]

The restacking of $KCa_2Nb_3O_{10}$ from monolayers makes it possible to increase the specific surface area from 3 to 27 $m^2\ g^{-1}$, which leads to a proportional (8.7-fold) gain in activity in photocatalytic hydrogen evolution from aqueous methanol (10 vol.%) under UV light irradiation.[97] The optimal amount of platinum, which is used as a cocatalyst, increases in proportion from 0.1% to 1%. Under these conditions, reassembled $KCa_2Nb_3O_{10}$ only slightly exceeds titania in photocatalytic activity.

Noteworthy, of the restacked niobates, triple-layered oxides have photocatalytic activities one order of magnitude higher than those of double-layered oxides, just as the precursor unsplit compounds.[167]

VI.3. Effect of Ca^{2+} replacement in $ACa_2Nb_3O_{10}$ on photocatalytic activity

The replacement of calcium atoms in $RbCa_2Nb_3O_{10}$ by lead induces [168] a bathochromic shift of the optical absorption edge ($E_g \approx 2.6$ eV) and thereby to the appearance of photocatalytic activity under visible light irradiation ($\lambda > 420$ nm).[169] Once $RbPb_2Nb_3O_{10}$ is protonated, its activity in photocatalytic hydrogen evolution from aqueous methanol (17 vol%) increases due to the acquired intercalation ability. Photoreduction from $Pt(NH_3)_4^{2+}$ and $PtCl_6^{2-}$ complex ions was used for loading $HPb_2Nb_3O_{10}$ with platinum. In the former, a positively charged platinum complex entered the interlayer space due to an ion-exchange reaction and platinum particles were formed as a result of irradiation. In the latter, platinum particles deposited only on the surface of layered oxide. For this reasons, when $Pt(NH_3)_4Cl_2$ was used to modify $HPb_2Nb_3O_{10}$, the photocatalytic activity was four times greater than when H_2PtCl_6 was used. Chromium doping increased the $HPb_2Nb_3O_{10}$ activity in photocatalytic hydrogen evolution from aqueous methanol (20 vol.%) by a factor of 1.6 at $\lambda > 400$ nm.[170]

Thus, the replacement of an alkaline-earth metal in a triple-layered Dion–Jacobson phase by lead is a promising method for producing photocatalysts that will be active in the visible range. Exfoliation of $HPb_2Nb_3O_{10}$, which is typical of its isostructural analogues, is of interest in this context.

Calcium cations in the $HCa_2Nb_3O_{10}$ structure can partially be replaced by lanthanum to slightly increase the photocatalytic activity in hydrogen evolution from aqueous methanol (10 vol.%).[171] Huang *et al.*[171] explained this by a reduction in charge density in the interlayer space, which makes the intercalation of reactants into the $H_{1-x}La_xCa_{2-x}Nb_3O_{10}$ structure easier than into the $HCa_2Nb_3O_{10}$ structure. Doping $KSr_2Nb_3O_{10}$ with chromium provides some increase in photocatalytic activity.[172] The optimal x value in $K_{1+2x}Sr_2Nb_{3-x}Cr_xO_{10}$ is 0.0125; greater chromium levels cause a strong progressive decline in activity.

VI.4. Photocatalysts produced by exfoliating $HCa_2Nb_3O_{10}$

Layered oxide $KCa_2Nb_3O_{10}$ prepared by routine solid-phase synthesis has no activity in photocatalytic water splitting even when loaded with the cocatalyst RuO_x. The exfoliation and restacking technique can be used to incorporate cocatalyst species in between perovskite layers; this can be helpful to achieve the evolution of stoichiometric hydrogen and oxygen amounts from water under exposure to the UV light. For example, the restacking of $Ca_2Nb_3O_{10}^-$ nanosheets in aqueous KOH in the presence of Ruthenium Red (a trinuclear ruthenium complex) involves the capture of complex molecules into the interlayer space. Subsequent heating or UV illumination gives rise to the formation, in the interlayer space, of RuO_x species, which perform as an oxygen evolution catalyst. The thus-prepared photocatalyst splits water under UV light. The replacement of potassium by sodium ions increases the activity presumably due to facilitating the hydration of the interlayer space.[159]

Hata *et al.*[163] used a similar approach to incorporate Rh_2O_3 nanoparticles into the interlayer space of $KCa_2Nb_3O_{10}$, which resulted in a twofold increase in activity in photocatalytic hydrogen evolution from aqueous methanol (10 vol%) solution. The authors[163] failed to accomplish photocatalytic water splitting. Noteworthy, the photocatalytic activity of restacked layered $HCa_2Nb_3O_{10}$ did not differ strongly from the activity of disperse perovskite nanosheets.[160]

VI.5. Photocatalytic activity of layered tantalates. Role of intercalation in photocatalysis

Triple-layered tantalates of composition $MCa_2Ta_3O_{10}$ (M = Cs, Na or H) are photocatalytically active in UV-light driven water splitting reaction.[173] Band gaps in these compounds are slightly wider than in similar niobates, and vary in the range from 4.1 to 4.3 eV depending on the interlayer cation. When $NaCa_2Ta_3O_{10}$ is exposed to water, water molecules are intercalated into its interlayer space (1.86 molecules per formula unit), whereas $CsCa_2Ta_3O_{10}$ is completely stable to hydration. It is likely for this reason that $NaCa_2Ta_3O_{10}$ is superior to $CsCa_2Ta_3O_{10}$ in photocatalytic activity, which is especially prominent after loading with cocatalyst NiO_x (0.5 mass %) (Table 12). The quantum efficiency for water splitting over $NaCa_2Ta_3O_{10}/NiO_x$ is $\sim 5\%$.

The nickel loading procedure comprises reductive treatment with hydrogen at 500 °C; the $HCa_2Ta_3O_{10}$ protonated phase is likely to experience irreversible dehydration at this temperature. If so, the values of $HCa_2Ta_3O_{10}/NiO_x$ photocatalytic activity reported by Machida *et al.*[173] actually refer to a phase of another composition.

Table 12. Photocatalytic activity of $MCa_2Ta_3O_{10}$ (M = Cs, Na, H) tantalates in the reaction of water splitting before and after loading with 0.5% NiO_x.[173]

Sample	Gas evolution rate /μmol h^{-1}	
	H_2	O_2
$CsCa_2Ta_3O_{10}$	7.6	2.2
$NaCa_2Ta_3O_{10}$	12.2	7.6
$HCa_2Ta_3O_{10}$	2.6	0.7
$CsCa_2Ta_3O_{10}/NiO_x$	23.9	10.3
$NaCa_2Ta_3O_{10}/NiO_x$	308.4	157.7
$HCa_2Ta_3O_{10}/NiO_x$	22.2	5.2

Note. Parameters of the experiment: 0.2 g of the catalyst per 200 m^3 of water, a high-pressure mercury lamp (400 W), an internal radiation unit, a closed gas circulation system, argon pressure 150 mm Hg.

Isotope-exchange experiments using IR spectroscopy showed that, when a $NaCa_2Ta_3O_{10}\cdot x\,H_2O$ sample was placed in heavy water, the replacement of H_2O in the interlayer space by D_2O from solution occurred very slowly. However, the exchange was accelerated under UV light irradiation. The isotope analysis of the hydrogen evolved in the photocatalytic reaction from a $CsCa_2Ta_3O_{10}$ slurry in D_2O, showed that the ratios $HD:D_2$ and $H_2:D_2$ increased with time to become 0.1 and 0.02, respectively, after a steady state was acquired, due to the presence of minor H_2O. When $NaCa_2Ta_3O_{10}\cdot x\,H_2O$ slurry in D_2O was irradiated, the ratios $HD:D_2$ and $H_2:D_2$ decreased with time to become 0.28 and 0.03 after a steady state was acquired; these values are about two times the respective values for $CsCa_2Ta_3O_{10}$. This signifies that interlayer H_2O molecules of layered $NaCa_2Ta_3O_{10}$ participate in the photocatalytic process. Unfortunately, the experiments give no answer to the question of whether water splitting occurs in the interlayer space or on the oxide surface where water appears as a result of outward diffusion from the crystal bulk. A piece of evidence for the second scenario is that $NaCa_2Ta_3O_{10}$ surface loading by NiO_x species, which are treated as hydrogen evolution sites, increases the photocatalytic activity of the sample by one order of magnitude.

Mitsuyama *et al.*[86] studied the photocatalytic activity of a series of layered tantalates $MCa_2Ta_3O_{10}$ (M = Li, Na, K, Rb or Cs). The ratio of UV light-driven water splitting rates over modified NiO_x samples was slightly different from the value obtained by Machida *et al.*,[173] which is one more illustration of the poor reproducibility of photocatalytic experiments even in one team of researchers. In the series of tantalates under consideration, only $NaCa_2Nb_3O_{10}$ was capable of intercalating water into the interlayer space (two water molecules per formula unit); however, the maximal activity was observed for a $LiCa_2Nb_3O_{10}$ sample. The researchers cited[173] hypothesized that water intercalation into $LiCa_2Nb_3O_{10}$ is controlled by kinetic factors, and if these factors are overcome, the resulting hydrated phase will acquire an even greater photocatalytic activity. Indeed, hydrothermal treatment at 160 °C for 12 h yielded a $LiCa_2Nb_3O_{10}/NiO_x$ sample having water molecules in the interlayer space (up to 0.64 water molecules per formula unit), whose photocatalytic activity was twice as high as the activities of unhydrated samples (Table 13).

Table 13. Photocatalytic activities of $MCa_2Ta_3O_{10}$ (M = Li, Na, K, Rb, Cs) tantalates.[86]

Sample	Gas evolution rate /μmol h^{-1}	
	H_2	O_2
$LiCa_2Ta_3O_{10}\cdot x H_2O$ [a]	708	333
$LiCa_2Ta_3O_{10}$	356	194
$NaCa_2Ta_3O_{10}\cdot x H_2O$	293	162
$KCa_2Ta_3O_{10}$	177	81
$RbCa_2Ta_3O_{10}$	180	91
$CsCa_2Ta_3O_{10}$	89	53

Note. All samples were modified with 0.5% NiO_x. Parameters of the experiment: 0.2 g of the catalyst per 200 ml of water, a high-pressure mercury lamp (400 W), an internal radiation unit, a closed gas circulation system. [a] The sample was prepared by hydrothermal treatment.

Hydrothermal treatment at higher temperatures reduced the photocatalytic activity, presumably due to the oxidation of the cocatalyst. There is no direct correlation between the photocatalytic activity and the amount of water intercalated into samples treated under different conditions. Intriguingly, the activity-enhancing effect was achieved only when the hydrothermally treated sample had been modified with NiO_x. When unmodified $LiCa_2Ta_3O_{10}$ was treated in the same way, only a decay in activity was observed despite hydration.

Hydrothermal treatment is not the only way to provide the hydration of interlayers in $LiCa_2Ta_3O_{10}$ structure; partial replacement of Li^+ by Na^+ cations can also be helpful in this regard.[174] When the relative sodium content is 0.77, the degree of hydration corresponds to a $NaCa_2Ta_3O_{10}$ phase and the photocatalytic activity has a maximal value of this solid solution series, approaching the highest value obtained by Mitsuyama *et al.*[86] for a hydrothermally treated $LiCa_2Ta_3O_{10}$ sample. The authors explained the high activity of the initial $LiCa_2Ta_3O_{10}$ phase by structural factors: the distortion of tantalum–oxygen octahedra gives rise to a dipole moment, and the dipole moment promotes the spatial separation of electron and holes. At the same time, the high activity of $NaCa_2Ta_3O_{10}$ is due to the hydration of the interlayer space, so the layered oxide $Li_{0.23}Na_{0.77}Ca_2Ta_3O_{10}$ has the best combination of the two factors. As the replacement of K^+ by Na^+ cations in $KCa_2Ta_3O_{10}$ progresses, the photocatalytic activity increases monotonically in response to increasing degree of hydration.

Huang *et al.*[175] studied the activity along the $KSr_2Ta_xNb_{3-x}O_{10}$ and $HSr_2Ta_xNb_{3-x}O_{10}$ (x = 0, 1, 1.5, 2 or 3) solid solution series in photocatalytic hydrogen evolution from methanol solution (10 vol.%). $HSr_2Nb_3O_{10}$ showed the highest activity in the absence of cocatalysts; after platinum species were intercalated into the interlayer space, $HSr_2TaNb_2O_{10}$ solid solution did this with a quantum efficiency of 2.7%.

The incorporation of ZnS and PbS species into interlayers also increased the photocatalytic activities of $HSr_2Nb_3O_{10}$ and $HSr_2TaNb_2O_{10}$.[176] The incorporation was accomplished by consecutive intercalation of n-hexylamine, ion exchange for Zn^{2+} and Pb^{2+} and hydrogen sulfide treatment.

Triple-layered tantalates are subject to exfoliation, as niobates, and this can be used to create efficient photocatalytic systems. For example, rhodium-modified nanolayers produced by the exfoliation of nitrogen-doped $HCa_2Ta_2O_{9.7}N_{0.2}$ showed the photocatalytic water splitting activity [177] that was one order of magnitude higher than for an unexfoliated sample.

VI.6. Photocatalytic activities of $ALnTa_2O_7$ double-layered tantalates

Double-layered tantalates of the family $ALnTa_2O_7$ (A = Cs, Rb, Na or H; Ln = La, Pr, Nd or Sm) feature photocatalytic activity in UV radiation-induced water splitting.[87, 178–180] The band gap energy in this series of compounds depends on the lanthanide and is 3.9, 3.6, 4.2 and 4.2 eV for A = La, Pr, Nd and Sm, respectively. The photocatalytic activity also depends appreciably on the lanthanide and takes a maximal value for $RbNdTa_2O_7$ (Table 14).

Table 14. Photocatalytic activities of $RbLnTa_2O_7$ (Ln = La, Pr, Nd, Sm) tantalates.[180]

Sample	E_g /eV	Gas evolution rate /μmol h^{-1}	
		H_2	O_2
$RbLaTa_2O_7$	3.9	1.2	0.6
$RbPrTa_2O_7$	3.6	0.9	0.1
$RbNdTa_2O_7$	4.2	47	25.3
$RbSmTa_2O_7$	4.2	10.6	5.7

Note. Parameters of the experiment: 0.2 g of the catalyst per 200 ml of water, a high-pressure mercury lamp (400 W), an internal radiation unit, a closed gas circulation system, argon pressure: 150 mm Hg.

This trend can in part be interpreted, based on quantum-chemical calculations, by that the lanthanide 4*f* orbitals are partially delocalized and participate in the valence band and conduction band thereby influencing the positions of band edges, the densities of states, and the mobilities of photogenerated charge carriers.[180] The hydration capability of $ALnTa_2O_7$ double-layered tantalates is determined by the alkali metal A. Of the series of double-layered tantalates under consideration, only $NaLnTa_2O_7$ compounds are capable of reversibly intercalating water into their interlayer spaces. In this case, however, unlike triple-layered Ruddlesden–Popper and Dion–Jacobson phases, the hydration of interlayers does not noticeably increase the photocatalytic activity, and the maximal activity is observed in $RbNdTa_2O_7$ and $CsNdTa_2O_7$ samples, which do not intercalate water under ambient temperature and pressure.[64, 87, 181] This difference can be assigned to the different electronic structures of double-layered and triple-layered Dion–Jacobson phases. For triple-layered tantalates, the orbitals of terminal oxygen atoms that surround the interlayer space are the major contributors to the valence band. For double-layered tantalates, these orbitals lie 1 eV below the valence band top. Thus, the interaction of photogenerated holes with intercalated molecules in two-layer tantalates is hindered.[173] This example well illustrates the fact that the capability to intercalate reactant molecules

into the interlayer space is not always a favourable factor for the photocatalytic activity of layered oxides.

VII. Aurivillius phases

VII.1. Structure and most important properties

Recently Aurivillius phases have extenseively been studied as photocatalysts in view of their capability to absorb visible light. The major subjects of studies include monolayered (isostructural to Bi_2MoO_6, Bi_2WO_6),[128] double-layered ($PbBi_2Nb_2O_9$) and triple-layered ($Bi_4Ti_3O_{12}$) Aurivillius phases, the structures of which are visualized in Fig. 11. The Bi_2WO_6 structure is an analogue of the Bi_2MoO_6 structure.[182] Aurivillius phases typically have a considerably distorted structure of perovskite layers; the distortion consists of a rotation of metal–oxygen octahedra and is responsible for the lowering of crystal-lattice symmetry from tetragonal to orthorhombic.

Intercalation of molecules into the interlayer space, which is an important factor for the properties of Ruddlesden–Popper and Dion–Jacobson phases, is not typical of Aurivillius phases. Protonation of Aurivillius phases is possible in some cases; however, the products of this reaction are not Aurivillius phases, but rather Ruddlesden–Popper phases, as $Bi_2O_2^{2+}$ structural units in the interlayer space are replaced by protons.[23] In the context of photocatalysis, this, as a rule, results in an increase in photocatalytic activity in the UV range with a simultaneous decline in activity in the visible range due to the increase in band gap energy of the layered oxide.[186, 187] Meanwhile, the main strength of Aurivillius phases as photocatalysts consists just in their capability to absorb visible light.

VII.2. Absorption of visible light by Aurivillius phases

One way to decrease the band gap energy of an oxide photocatalyst in order to make it capable of absorbing visible light is to dope it with metals with s^2 electronic configuration which would contribute to the valence band together with oxygen atoms.[188] This is just the case in photocatalysts comprising Aurivillius phases, as all of them contain Bi^{3+}, whose electronic configuration is s^2.

For Bi_2WO_6 (E_g = 2.7–2.8 eV), density functional quantum chemical calculations showed that the absorption of visible light is associated with the transiiotn of an electron from the valence band, which is formed by Bi6s and O2p orbitals, to the conduction band, which is formed by W5d orbitals.[189] In $ABi_2Ta_2O_9$ (A = Ca, Sr or Ba), the valence band is formed by O2p, Ta5d and Bi6s orbitals and the conduction band is formed by Bi6p, Ta5d and O2p orbitals.[190] These compounds do not absorb visible light; however, they have smaller band gap energies than the ATa_2O_6 (A = Ca, Sr or Ba) bismuth-free tantalates. In the latter, the conduction band and valence band are formed by Ta5d and O2p orbitals, respectively. The data shown in Table 15 imply that the decrease in band gap energy in going from binary tantalates to Aurivillius phases averages ~0.3–0.7 eV. This is explained by the hybridization of occupied bismuth 6s orbitals with oxygen 2p orbitals to heighten the valence band top.

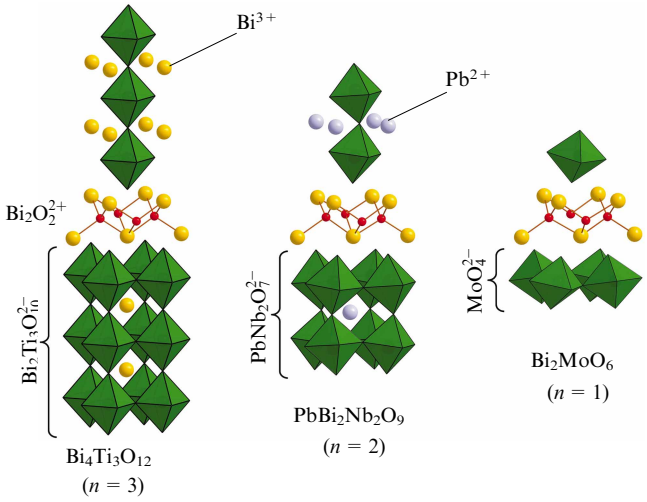


Figure 11. Structures of Aurivillius phases $Bi_4Ti_3O_{12}$, $PbBi_2Nb_2O_9$ and Bi_2MoO_6.[182–185]

The electronic structure of $ABi_2Nb_2O_9$ (A = Ca, Sr or Ba) niobates, which are Aurivillius phases, is similar to the electronic structure of the corresponding tantalates. The valence band is formed by O2p, Nb4d and Bi6s orbitals, and the conduction band is formed by Bi6p, Nb4d and O2p orbitals.[191] The niobates have slightly narrower band gaps compared to their isostructural tantalates, where E_g decreases as the alkaline-earth metal radius increases (Table 15).

The observed effect of heightening the valence band top is enhanced by increasing bismuth content of the complex oxide. This trend can be seen in $Bi_2LaSrTi_2TaO_{12}$ and $Bi_3SrTi_2TaO_{12}$, which are triple-layered Aurivillius phases.[192] The values of E_g for these compounds are 3.48 and 3.32 eV, respectively. In this case, the unoccupied Ti3d and Ta4d orbitals form the conduction band and the O2p and Bi6s hybridized orbitals form the valence band. The hybridization is enhanced as the bismuth content increases, which is manifested in a 0.16 eV narrowing of the band gap.

A still more significant narrowing of the band gap can be accomplished by doping the layered oxide structure (in addition to bismuth) with doubly charged lead, which also

Table 15. Band gap energies of tantalate and niobate Aurivillius phases and binary tantalates.[190, 191]

Binary tantalate	E_g/eV	Tantalate Aurivillius phase	E_g/eV	Niobate Aurivillius phase	E_g/eV
$CaTa_2O_6$	4.0	$CaBi_2Ta_2O_9$	3.67	$CaBi_2Nb_2O_9$	3.46
$SrTa_2O_6$	4.4	$SrBi_2Ta_2O_9$	3.64	$SrBi_2Nb_2O_9$	3.43
$BaTa_2O_6$	4.1	$BaBi_2Ta_2O_9$	3.52	$BaBi_2Nb_2O_9$	3.30

Table 16. Photocatalytic activity of individual Aurivillius phases prepared by various methods.

Photocatalyst synthesis method	Model reaction	Parameters of the experiment	Result		Ref.
			gain in activity [a]	parameters	
		Photocatalyst Bi_2WO_6			
Sol–gel synthesis with albumin (according to increase in S_{sp}) as the biotemplate, $S_{sp} = 3.5\ m^2\ g^{-1}$ (under the same conditions but without albumin, $S_{sp} = 1.2\ m^2\ g^{-1}$)	Degradation of rhodamine B (5 mg litre^{-1})	$c_{cat} = 1$ g litre^{-1}, Xe 300 W	2.8 with albumin	–	209
Microspheres of Bi_2WO_6 nanoparticles, $S_{sp} = 42.8\ m^2\ g^{-1}$	Degradation of rhodamine B (5×10^{-5} mol litre^{-1})	$c_{cat} = 1$ g litre^{-1}, Xe 500 W, $\lambda > 400$ nm	No degradation	–	216
Hydrothermal synthesis at pH 2, 6, 10	Degradation of rhodamine B (10^{-5} mol litre^{-1})	$c_{cat} = 1$ g litre^{-1}, Xe 450 W	3.2 following pH decrease from 10 to 2 (according to increase in S_{sp})	pH 2, $S_{sp} = 31.0$, $k = 0.038$; pH 6, $S_{sp} = 20.2$, $k = 0.018$; pH 10, $S_{sp} = 6.9$, $k = 0.012$	215
Hydrothermal synthesis, microdiscs, $S_{sp} = 26.1$, $S_{sp}^{as} = 0.64\ m^2\ g^{-1}$	Degradation of rhodamine B (10^{-5} mol litre^{-1})	$c_{cat} = 1$ g litre^{-1}, Xe 500 W	~ 20	–	210
Hydrothermal synthesis, $S_{sp} = 16.3$, $S_{sp}^{as} = 0.64\ m^2\ g^{-1}$	Degradation of rhodamine B (10^{-5} mol litre^{-1})	$c_{cat} = 0.5$ g litre^{-1}, Xe 500 W, $\lambda > 400$ nm	6.7	$k = 0.020$, $k^{as} = 0.003$	211
Hydrothermal synthesis, nanoplates $S_{sp} = 5.63$, $S_{sp}^{as} = 0.6\ m^2\ g^{-1}$	Reduction of CO_2 in the gas phase ($p = 1$atm)	$m_{cat} = 0.1$ g, reactor area 4.2 cm^2, reactor volume 230 ml, +1 ml of water Xe 500 W, $\lambda > 420$ nm	24.4	$\omega = 1.1$ μmol g^{-1} h^{-1}, $\omega^{as} = 0.045$ μmol g^{-1} h^{-1}, see [b]	217
		Photocatalyst $Bi_4Ti_3O_{12}$			
Solid-phase method, $S_{sp} = 3.5\ m^2\ g^{-1}$	Degradation of 4-chlorophenol (1.25×10^{-5} mol litre^{-1})	$c_{cat} = 0.5$ g litre^{-1}, Hal 500 W, $\lambda > 420$ nm	–	$k = 0.0024$	218
	Degradation of microcystin-RR (0.4 g litre^{-1}),	$c_{cat} = 0.4$ g litre^{-1}, Hal 500 W, $\lambda > 420$ nm	–	$x \approx 100\%$ in 18 h; without a catalyst $x \approx 5\%$	218
Peroxide complex method	Degradation of rhodamine B (10 mg litre^{-1})	$c_{cat} = 0.75$ g litre^{-1}, Hg (m) 400 W	1.8 on going from the synthesis temperature of 800 °C to 900 °C owing to increase in the crystallinity	$S_{sp} = 2.6$, $k = 0.0078$; $S_{sp} = 1.8$, $k = 0.0140$	219
Hydrothermal synthesis at pH of 1 to 14	Degradation of rhodamine B (10^{-5} mol litre^{-1})	$c_{cat} = 1$ g litre^{-1}, Xe 500 W, $\lambda > 400$ nm	Increase with decreasing the synthesis pH (according to the increase in S_{sp})	pH 1, $S_{sp} = 48.8$, $x = 93\%$; pH 14, $S_{sp} = 7.1$, $x = 72\%$ in 360 min	214

Table 16 (continued).

Photocatalyst synthesis method	Model reaction	Parameters of the experiment	Result		Ref.
			gain in activity [a]	parameters	
		Photocatalyst $Bi_4Ti_3O_{12}$			
Hydrothermal synthesis, particles of various morphology	Degradation of Methyl Orange (10^{-5} mol litre^{-1})	c_{cat} = 1 g litre^{-1}, Xe 300 W, $\lambda > 420$ nm	Increase according to the increase in S_{sp}	S_{sp} = 53.6, k = 0.0036; S_{sp} = 74.2, k = 0.0042; S_{sp} = 90.5, k = 0.0078; for TiO_2/N S_{sp} = 31.8, k = 0.0019	212
		Modifier Bi_2MoO_6			
Co-precipitation under sonication	Degradation of rhodamine B (5 mg litre^{-1})	c_{cat} = 1 g litre^{-1}, Xe 5600 K, 85 000 lx	7–18 (according to the increase in S_{sp})	T = 450 °C, k = 0.007, S_{sp} = 0.4; T = 400 °C, k = 0.009, S_{sp} = 4.2; T = 350 °C, k = 0.018, S_{sp} = 11.9, $k^{as} \approx 0.001$	213

Note. The following notations are used: S_{sp} is the specific surface area /m^2 g^{-1}, c_{cat} and m_{cat} are the catalyst concentration and mass, respectively, Hal is the halogen lamp, Hg (m) is the medium-pressure mercury lamp; k is the pseudo-first-order rate constant /min^{-1}; x is the degree of substrate conversion; ω is the reaction rate; values with the superscript 'as' refer to the Aurivillius phases obtained by the solid-phase method. [a] The factor by which the photocatalytic activity is greater than in the sample obtained by the solid-phase method. [b] Apart from S_{sp} the particle morphology plays a role: the plate surface corresponds to the {001} face on which CO_2 dissociation is easier.

has the s^2 electronic configuration. This can well be seen for $PbBi_2Nb_2O_9$, where the valence band is formed of O2p orbitals, which interact both with Bi6s orbitals and with Pb6s orbitals.[193] This effect causes an even greater heightening of the valence band top, and the band gap of this compound is as narrow as 2.88 eV, *i.e.*, 0.42 eV narrower than in the analogue that contains barium instead of lead atoms (see Table 15). Due to this, $PbBi_2Nb_2O_9$ doped with 0.1% Pt, is photocatalytically active under visible light irradiation; specifically, it shows 0.95% quantum efficiency in the reaction of hydrogen evolution from methanol solution (15 vol.%), and its quantum efficiency in the reaction of oxygen evolution from 0.05 M silver nitrate solution at $\lambda > 420$ nm is 29%.[184] Noteworthy, the incorporation of lead cations into the structure narrows the band gap not only in Aurivillius phases, but also in other classes of layered oxides.[169, 188]

VII.3. Photocatalytic activity of unmodified Aurivillius phases. Correlation between the photocatalytic activity and specific surface area

Most studies into the photocatalytic properties of Aurivillius phases now underway involve the development of new synthetic methods (primarily sol–gel and and solvothermal methods) that would make it possible to control particle morphology and to increase specific surface areas to the maximal possible extent compared to the routine high-temperature solid-phase synthesis. The major focus of those studies is on binary oxides Bi_2MoO_6,[189, 194–198] Bi_2WO_6[189, 194, 199–203] and $Bi_4Ti_3O_{12}$ (Refs 204–206) and some ternary oxides.[207, 208] The main inference from the studies consists in that the increasing specific surface areas and crystallinities increase the photocatalytic activity. This trend can be traced in recent studies into the photocatalytic activity of individual (unmodified) Aurivillius phases;[209–215] the results of these studies are shown in Table 16.

Apart from the specific surface area, one more factor that can influence the photocatalytic activity is the type of crystal plane that primarily contacts the reaction medium as shown by Zheng *et al.*[198] for Bi_2WO_6. The researchers[198] used a hydrothermal method to prepare three samples that morphologically differed from each other: large platelets, small platelets and various nanoparticles. The specific surface areas increased in this series of samples while the photocatalytic activities decreased. The sample that consisted of large platy particles whose sufrace coincided with the crystalllographic plane {010} showed the highest activity. The authors[198] explained the enhanced catalytic activity of this facet by the distortion of molybdenum–oxygen octahedra and the attendant high surface density of oxygen defects and structural vacancies, which facilitate the generation of OH and OOH radicals.

VII.4. Photocatalytic processes involving Aurivillius phases

The most popular model reactions in studies of the photocatalytic properties of Aurivillius phases are the reactions of light-driven degradation of organic dyes (Rhodamine B, Methyl Orange and Methylene Blue) in aqueous solution. The popularity of these reactions is due primarily to the ease of experimentation. As mentioned above (see Section II), however, when a dye is used as a substrate, its degradation is frequently non-photocatalytic, specifically over Aurivillius phases.[195, 197] Therefore, many of the surveyed studies may relate to photocatalysis only circumstantially, especially if the authors confined themselves to measurements of dye discoloration rates and did not analyze reaction products.

Studies of the mechanism of Rhodamine B degradation over Bi_2MoO_6 under visible light ($\lambda > 420$ nm) showed that the first reaction steps involve the consecutive splitting of four ethyl groups to form an intermediate, which is then oxidized.[220] By the moment when the Rhodamine is completely degraded, the organic carbon content of the system is reduced by as little as $\sim 30\%$. This well illustrates the fact that, when the photocatalytic method is used, the discoloration of the dye solution is not an indication of the complete purification of water.

Aurivillius phases were shown to have activity in some other photocatalytic reactions under visible light: the degradation of phenol,[221–225] 4-chlorophenol,[218] 4-nitrophenol[226] and microcystin-RR[218] in aqueous solutions, and the reduction of nitrobenzene to aniline in methanol solution.[227] Aurivillius phases were shown to be useful in the vapour-phase degradation of benzene,[228] toluene[229] and acetaldehyde.[230] The conditions of the relevant experiments and selected results can be found in Table 16 and in other tables of this survey.[228–246]

The report by Zhou *et al.*,[217] who accomplished CO_2 reduction to methane under visible light ($\lambda > 420$ nm), deserves special attention. The photocatalyst they used was a hydrothermally prepared Bi_2WO_6 sample. In methane formation rates (1.1 μmol g^{-1} h^{-1}), this sample was 24.4 times better than a sample prepared by solid-phase synthesis. Apart from different specific surface areas of the samples, the authors[217] assigned the effect to particle morphology: in hydrothermally prepared platelike particles, the surfaces concided with the crystallographic plane {001}, which is the best for CO_2 dissociation according to quantum chemical calculations.

VII.5. Effect of doping on the photocatalytic activity of Aurivillius phases

Doping a semiconductor with donor or acceptor components is a well-known route to modify the electronic structure in order to generate n- or p-type conduction. Kim *et al.*[247] used this route to modify a $PbBi_2Nb_2O_9$ photocatalyst. They prepared samples where niobium atoms were partially replaced by tunsgten (donor) or by titanium (acceptor) and studied the photocatalytic activity of these samples in the reactions of hydrogen and oxygen evolution from water in the presence of methanol and silver nitrate, respectively.

The data shown in Table 17 imply that titanium (acceptor) doping reduced the photocatalytic activity of $PbBi_2Nb_2O_9$; tungsten (donor) doping, in contrast, increased the photocatalytic activity so that the photocatalytic activity *versus* tungsten content had a peak when the tungsten-for-niobium substitution level was 7.5%. The authors[247] related the increase in photocatalytic activity induced by additions of donors to the compression of the near-surface transition layer within the semiconductor and an increased bent of the bands in this region, which leads to a more efficient electron–hole separation. The decline in photoactivity upon a further

Table 17. Photocatalytic activity of tungsten- or titanium-doped $PbBi_2Nb_2O_9$.[247]

Catalyst	E_g /eV	H_2 evolution (see [a])		O_2 evolution (see [b])	
		rate /μmol g^{-1} h^{-1}	QE (%) (see [c])	rate /μmol g^{-1} h^{-1}	QE (%) (see [c])
$PbBi_2Nb_{1.8}W_{0.2}O_9$	2.74	11.7	1.45	602	33
$PbBi_2Nb_{1.85}W_{0.15}O_9$	2.74	15.3	1.92	631	35
$PbBi_2Nb_{1.9}W_{0.1}O_9$	2.75	9.1	1.13	580	32
$PbBi_2Nb_2O_9$	2.88	7.6	0.95	520	29
$PbBi_2Nb_{1.9}Ti_{0.1}O_9$	2.91	2.8	0.35	430	24
$TiO_{2-x}N_x$	2.73	Traces	0	221	14

Note. All samples were modified with 0.1% Pt. Parameters of the experiment: 0.3 g of the catalyst per 200 ml of the solution, Xe (450 W, $\lambda > 420$ nm). [a] From methanol solution (15 vol.%). [b] From 0.05 M $AgNO_3$ solution. [c] QE stands for quantum efficiency.

Table 18. Photocatalytic activity of doped Aurivillius phases.

Dopant		Model reaction	Parameters of the experiment	Result			Ref.
ion	concentration (mol.%)			gain in activity [a]	k^0	k^d	
			Photocatalyst Bi_2WO_6				
Er^{3+}	0.6	Rhodamine B degradation (10^{-5} mol $litre^{-1}$)	c_{cat} = 1 g $litre^{-1}$, Xe 500 W, $\lambda > 290$ nm	2.4	0.042	0.102	221
		Phenol degradation (20 mg $litre^{-1}$)	c_{cat} = 1.67 g $litre^{-1}$, Xe 500 W, $\lambda > 290$ nm	6	0.001	0.006	221
		The same	c_{cat} = 1.67 g $litre^{-1}$, LED 3 W, λ = 465 nm	Activity appears	0	0.0002	221
Zr^{4+}	3	Rhodamine B degradation (10^{-5} mol $litre^{-1}$)	c_{cat} = 1 g $litre^{-1}$, Xe 500 W, $\lambda > 420$ nm	3.8	0.06	0.23	222
		Phenol degradation (20 mg $litre^{-1}$)	c_{cat} = 1 g $litre^{-1}$, Xe 500 W, $\lambda > 420$ nm	6.9	0.0012	0.0083	222
Sn^{2+}	2	Rhodamine B degradation (5×10^{-6} mol $litre^{-1}$)	c_{cat} = 1 g $litre^{-1}$, W 300 W	No changes	–	–	231
Fe^{3+}	0.5	Methylene Blue degradation (2×10^{-5} mol $litre^{-1}$)	c_{cat} = 10 g $litre^{-1}$, Hal 50 W	3.6 S^0_{sp}= 14.4, S^d_{sp}= 33.4 m^2 g^{-1}	0.0032	0.0116	232
			Photocatalyst Bi_2MoO_6				
Gd^{3+}	25	Rhodamine B degradation (10 mg $litre^{-1}$)	Hal 300 W, $\lambda > 420$ nm	2.8 S^0_{sp}= 2.8, S^d_{sp}= 7.2 m^2 g^{-1}	0.0044	0.0122	233
Ho^{3+}	25	The same	Hal 300 W, $\lambda > 420$ nm	1.8 S^d_{sp}= 4.6 m^2 g^{-1}	0.0044	0.0078	233
Yb^{3+}	25	"	Hal 300 W, $\lambda > 420$ nm	2 S^d_{sp}= 5.2 m^2 g^{-1}	0.0044	0.0091	233
W^{6+}	50	Rhodamine B degradation (10^{-5} mol $litre^{-1}$)	c_{cat} = 3.3 g $litre^{-1}$, Xe 500 W, $\lambda > 400$ nm	1.3 (x^0 = 64%, x^d = 86% in 80 min)	–	–	234

Note. Notations: LED is light-emitting diode, W 300 W is a tungsten lamp with a wattage of 300 W, superscripts '0' and 'd' refer to the undoped and doped Aurivillius phases, respectively. [a] The factor by which the photocatalytic activity of the doped sample is greater than in an undoped sample.

increase in tungsten concentration is likely to arise from the appearance of impurity phases. Tungsten addition gives rise to a bathochromic shift of the optical absorption edge, while titanium doping has the opposite effect.

Doping is known to shift the semiconductor absorption band to the visible range due to the generation of impurity levels inside the band gap. This approach was employed by Zhang *et al.*[248] to modify the Aurivillius phase $Bi_4Ti_3O_{12}$. This titanate has a band gap energy of 3.08 eV; its valence band and conduction band are built by O2p, Ti3d and Bi6s orbitals, and Ti3d and Bi6p orbitals, respectively. A partial substitution of chromium for titanium atoms results in the involvement of chromium 3d orbitals in the conduction band and the appearance of additional allowed states inside the band gap formed by the chromium 3d orbitals. The bathochromic shift of the absorption band of the photocatalyst is due to the possibility of electron transitions from these impurity levels to the conduction band. The activity of $Bi_4Ti_{2.6}Cr_{0.4}O_{12}$ in the reaction of visible light-driven photocatalytic hydrogen evolution from aqueous methanol (5 vol.%) was 1.6 times higher than for undoped $Bi_4Ti_3O_{12}$.

An interesting opportunity to expand the operative spectral range of an Aurivillius phase is offered by doping it with lanthanide ions, which can increase the radiation frequency. For example, a Bi_2WO_6/Er^{3+} (0.6 mol.%) sample featured activity in photocatalytic phenol degradation in aqueous solution under 465 nm radiation. Undoped Bi_2WO_6 was inactive under these conditions because of an insufficiently narrow band gap.[221]

Table 18 shows most important results of photocatalytic studies of doped Aurivillius phases obtained in the last five years.

VII.6. Composite photocatalysts containing Aurivillius phases

Aurivillius phases are of interest as potential components of two-photon photocatalytic systems due to their capability to absorb the visible light. For example, a two-photon composite photocatalyst was created on the basis of $PbBi_2Nb_2O_9$ where titanium substitutes for 10% niobium atoms to generate *p*-type conduction.[249] Tungsten nanoparticles were loaded onto the oxide surface, and then their surfaces were oxidized to WO_3 (which is an n-type semiconductor). In this way, a p–n junction was generated with a metallic tungsten interlayer: $WO_3/W/PbBi_2Nb_{1.9}Ti_{0.1}O_9$. When exposed to visible light, both the layered oxide $PbBi_2Nb_{1.9}Ti_{0.1}O_9$ and WO_3 absorb the light to generate electron–hole pairs. Electrons in WO_3 and holes in $PbBi_2Nb_{1.9}Ti_{0.1}O_9$ migrate to metallic tungsten and recombine, and the charge carriers that remain spatially separated can participate in oxidation and reduction reactions on the surface of the appropriate oxide. The composite sample was six times superior to $PbBi_2Nb_2O_9$/Pt (1%) in photocatalytic activity in the reaction of hydrogen evolution from methanol solution (15 vol.%), showing the 6% quantum efficiency at $\lambda > 420$ nm.

$PbBi_2Nb_2O_9$ was also used to create a composite photocatalyst: $PbBi_2Nb_{1.9}W_{0.1}O_9/CaFe_2O_4$.[250] In this case, the layered oxide was endowed with n-type conduction *via* tungsten doping, and $CaFe_2O_4$ is a p-type conductor. The composite sample had a threefold activity in photocatalytic acetaldehyde degradation compared to undoped $PbBi_2Nb_2O_9$. However, the tungsten doping alone gave a commensurate increase in photocatalytic activity in $PbBi_2Nb_2O_9$,[247] and it is not quite clear to which extent the gain in efficiency was directly due to the creation of composite (no activity comparison was carried out between the composite and $PbBi_2Nb_{1.9}W_{0.1}O_9$).

A similar two-photon scheme was accomplished for the layered oxide Bi_2WO_6 by loading its surface with Ag and AgBr particles.[202] Oxidation processes occurred on the Bi_2WO_6 surface, reduction processes occurred on the AgBr surface and silver served as the recombination site for electrons coming from Bi_2WO_6 and holes coming from

Table 19. Composite photocatalysts based on Aurivillius phases.

Photocatalyst		Model reaction	Parameters of the experiment	Result		Ref.
composition	S_{sp} /m^2 g^{-1}			gain in activity [a]	k	
Bi_2WO_6/10% Ag	$S_{sp}^{cc} = 19.5$	Degradation of Rhodamine B (10^{-5} mol litre^{-1})	$c_{cat} = 0.5$ g litre^{-1}, Xe 500 W, visible light	3	–	223
		Degradation of phenol, (10^{-5} mol litre^{-1})	$c_{cat} = 0.5$ g litre^{-1}, Xe 500 W, visible light	1.7	–	223
Bi_2MoO_6/0.15% Ag	$S_{sp}^{0} = 70$, $S_{sp}^{cc} = 55$	Reduction of nitrobenzene in methanol, ($8.13 \cdot 10^{-4}$ mol litre^{-1})	Xe 500 W, $\lambda > 400$ nm	4.5 (in 20 min, $\approx$97% of nitrobenzene is converted to aniline)	–	227
Bi_2MoO_6 /10% Ag	$S_{sp}^{0} = 18.7$, $S_{sp}^{cc} = 13.5$	Degradation of Rhodamine B (10^{-5} mol litre^{-1})	$c_{cat} = 1$ g litre^{-1}, $\lambda > 400$ nm	3.6	$k^{cc} = 0.047$, $k^{0} = 0.014$	235
Microspheres of Bi_2MoO_6 /2.1% Ag	$S_{sp}^{0} = 38$, $S_{sp}^{cc} = 40$	Degradation of Rhodamine B	$c_{cat} = 0.5$ g litre^{-1}, Xe 150 W, $\lambda > 420$ nm	3.8	$k^{0} = 0.0046$, $k^{cc} = 0.0175$	236
		of Methylene Blue,	$c_{cat} = 0.5$ g litre^{-1}, Xe 150 W, $\lambda > 420$ nm	3	$k^{0} = 0.0064$, $k^{cc} = 0.0190$	236
		of Methyl Orange (10 mg litre^{-1})	$c_{cat} = 0.5$ g litre^{-1}, Xe 150 W, $\lambda > 420$ nm	2.3	$k^{0} = 0.0042$, $k^{cc} = 0.0098$	236
Bi_2WO_6/0.3% Pt	–	Degradation of Methyl Orange (100 mg litre^{-1})	$c_{cat} = 0.4$ g litre^{-1}, Xe 300 W, $\lambda > 400$ nm	1.9	$k^{0} = 0.035$, $k^{cc} = 0.067$	237

Table 19 (continued).

Photocatalyst		Model reaction	Parameters of the experiment	Result		Ref.
composition	S_{sp} /m^2 g^{-1}			gain in activity [a]	k	
Bi_2WO_6/1% Pt/Cl^-	$S_{sp}^0 = 19.9$, $S_{sp}^{cc} = 32.4$	Degradation of toluene in the gas phase (25 ppm)	Xe 300 W, visible light	2.8	$k^{cc} = 0.152$	229
Bi_2WO_6/$BiVO_4$ (1 : 1)	$S_{sp}^{cc} = 2.69$	Degradation of Rhodamine B (10^{-5} mol litre^{-1})	c_{cat} = 1 g litre^{-1}, Xe 300 W, $\lambda > 420$ nm	3.3	$k^0 = 0.052$, $k^{md} = 0.045$, $k^{cc} = 0.171$	238
Bi_2WO_6/$CaWO_4$	–	Degradation of Rhodamine B (10^{-5} mol litre^{-1})	c_{cat} = 1 g litre^{-1}, Xe 300 W, $\lambda > 420$ nm	Almost no changes (composite sedimentation is faster)	–	239
Bi_2WO_6/Ag_3PO_4	$S_{sp}^{cc} = 37.2$	Degradation of phenol (20 mg litre^{-1})	c_{cat} = 1 g litre^{-1}, Xe 500 W, $\lambda > 420$ nm	~ 2	–	224
Bi_2WO_6/ 30 mol.% $ZnWO_4$	–	Degradation of acetaldehyde in the gas phase (250 ppm)	c_{cat} = 0.1 g litre^{-1}, BLB, I = 0.4 mW cm^{-2} 290 nm $< \lambda <$ 420 nm	1.5	$k^0 = 0.123$, $k^{cc} = 0.184$	230
$Bi_4Ti_3O_{12}$ nanofibres/ Bi_2MoO_6 nanosheets	$S_{sp}^0 = 10.9$, $S_{sp}^{cc} = 27.9$	Degradation of Rhodamine B (10 ppm)	c_{cat} = 1 g litre^{-1}, Xe 300 W, $\lambda > 400$ nm	3.5	$k^{cc} = 0.038$, $k^{mm} = 0.011$	240
$Bi_4Ti_3O_{12}$ nanofibres/ Bi_2MoO_6 nanosheets	$S_{sp}^0 = 10.9$, $S_{sp}^{cc} = 29.4$	The same	The same	8	$k^{cc} = 0.024$, $k^{mm} = 0.003$	240
$Bi_4Ti_3O_{12}$ nanofibres/ BiOCl nanosheets	$S_{sp}^{cc} = 119.4$	Degradation of Methyl Orange (10 ppm)	c_{cat} = 1 g litre^{-1}, Xe 300 W	1.5 ($x^{cc} = 62\%$, $x^{mm} = 96\%$ in 40 min)	–	226
		Degradation of 4-nitrophenol (10 ppm)	c_{cat} = 1 g litre^{-1}, Xe 300 W	1.4 ($x^{mm} = 63\%$, $x^{cc} = 91\%$ in 40 min)	–	226
Bi_2WO_6/58.5% AgJ	–	Degradation of Rhodamine B (10 mg litre^{-1})	c_{cat} = 2 g litre^{-1}, Xe 500 W, $\lambda > 420$ nm	~ 2	–	241
Bi_2MoO_6/SiO_2/Fe_3O_4	–	Degradation of Rhodamine B (10 mg litre^{-1})	c_{cat} = 1 g litre^{-1}, Xe 300 W, $\lambda > 400$ nm	(the composite can be fully separated from the solution by a magnet)	$k^0 = 0.022$, $k^{cc} = 0.029$	242
Bi_2WO_6/C (microspheres)	–	Degradation of benzene in the gas phase (94 ppm)	m_{cat} = 50 mg, flow type reactor v_o = 20 ml min^{-1}, Xe 500 W, $\lambda > 420$ nm	1.5 ($x^0 = 29.5\%$, $x^{cc} = 44.4\%$)	–	228
Bi_2MoO_6/graphene (1%)	–	Degradation of Methylene Blue (10^{-5} mol litre^{-1})	c_{cat} = 0.5 g litre^{-1}, Xe 500 W, $\lambda > 420$ nm, I = 31.2 mW cm^{-2}	3.7	$k^{mm} = 0.0037$, $k^{cc} = 0.0136$	243
Bi_2WO_6/g-C_3N_4 (70%)	–	Degradation of Methyl Orange (10 mg litre^{-1})	c_{cat} = 3 g litre^{-1}, Xe 500 W, $\lambda > 420$ nm	20.6	$k^{mm} = 0.0018$, $k^{cc} = 0.037$	244
Bi_2WO_6/g-C_3N_4 (33%)	–	Degradation of Methyl Orange (10 mg litre^{-1})	c_{cat} = 2 g litre^{-1}, Xe 300 W, $\lambda > 400$ nm	7.7	$k^{mm} = 0.0022$, $k^{cc} = 0.017$	245
Bi_2MoO_6/g-C_3N_4	–	Degradation of Rhodamine B) (1.25×10^{-5} mol litre^{-1})	c_{cat} = 0.8 g litre^{-1}, Xe 300 W, $\lambda > 400$ nm	5	$k^0 = 0.020$, $k^{md} = 0.041$, $k^{cc} = 0.108$	246
Bi_2MoO_6/copper phthalocyanine	–	Degradation of Rhodamine B (10^{-5} mol litre^{-1})	c_{cat} = 1 g litre^{-1}, Xe 500 W, $\lambda > 400$ nm	~ 1.5 ($x^{cc} \approx 100\%$ in 15 min)	–	225
	–	Degradation of Rhodamine B (10^{-5} mol litre^{-1})	c_{cat} = 1 g litre^{-1}, LED 3 W, λ = 620 nm	Activity appears ($x^0 \approx 0\%$, $x^{cc} = 91\%$ in 6 h)	–	225
	–	Degradation of phenol (20 mg litre^{-1})	c_{cat} = 1 g litre^{-1}, Xe 500 W, $\lambda > 400$ nm	Almost no changes	–	225

Note. The following notations are used: BLB is a black light lamp; g-C_3N_4 is the graphite-like carbon nitride; the superscripts '0', 'cc', 'mm' and 'md' stand for the initial Aurivillius phases, composite catalysts, mechamical mixture of the composite components and modifiers. [a] The factor by which composite photocatalytic activity is greater than that of the non-modified sample and/or the mechanical mixture of the components.

AgBr. This composite featured a higher activity compared to its individual components in photocatalytic pentachlorophenol degradation.

The design of composite photocatalysts has recently become most popular in research into the photocatalytic properties of Aurivillius phases. Table 19 shows most important results of relevant studies published in the last five years. The modifiers studied include metal particles (Ag[223, 227, 235, 236] and Pt[237]), semiconductor particles ($BiVO_4$,[238] $CaWO_4$,[239] Ag_3PO_4,[224] $ZnWO_4$,[230] BiOCl[226] and AgI[241]) and two-dimentional nanospecies [graphene[243] and g-C_3N_4 (Ref. 244–246)]. Most of the composite samples (except for $Bi_2WO_6/CaWO_4$) have photocatalytic activities 1.5–4 times greater than the initial Aurivillius phase or a mechanical mixture of the Aurivillius phase and a modifier. In all of the studies we cite here, the reason behind the higher activity of a composite photocatalyst compared to individual constituents is explained in the same terms: a combination of two phases that have different band gap (and Fermi level) positions gives rise to a contact potential difference, which favours the spatial separation of electrons and holes and thereby reduces the recombination probability. Therefore, it can be presumed that the hole-involving oxidation process occurs preferably on the surface of one component of the composite photocatalyst and the electron-involving reduction process occurs on the surface of the other.

An outstanding result was shown by a Bi_2WO_6 composite that contained graphite-like carbon nitride, a compound that has been actively studied as a photocatalyst in recent years.[251] That Bi_2WO_6/g-C_3N_4 composite exceeded a mechanical mixture of Bi_2WO_6 and g-C_3N_4 by more than 20 times.[244] More recently, Wang *et al.*[245] reported a gain of 7.7 times, likely due to the use of another radiation source and another light filter and to different compositions and preparation methods of the composites.

In the context of synthetic opportunities, noticeable is a composite of two Aurivillius phases, which represents $Bi_4Ti_3O_{12}$ nanofibres coated with Bi_2WO_6 nanosheets and which was produced hydrothermally; this composite was eight times superior in photocatalytic activity to a mechanical mixture of the components.[240] Further, due to its specific particle morphology (fibres about 10 μm long and ~150 nm in diameter), this photocatalyst was labile to sedimentation, and this can appear advantageous for water purification. A similar idea was put forward by Zhang *et al.*,[239] who did not observe increasing photocatalytic activity in $Bi_2WO_6/CaWO_4$ composite, but noticed decreasing sedimentation time. Hou *et al.*,[242] who created a Bi_2MoO_6 composite with SiO_2-coated magnetite, found a more elegant solution to the problem of separating photocatalyst particles from solution. Their photocatalyst was active in the visible and was easily separated from solution with a magnet. This is of obvious value for practice.

Zhang *et al.*[225] showed for Bi_2MoO_6 that an Aurivillius phase can be sensitized by dyes to expand the operative spectral range. When a copper phthalocyanine-modified Bi_2MoO_6 sample was used as the photocatalyst, Rhodamine B degradation was observed under exposure to 620 nm light. Degradation did not occur over the unsensitized photocatalyst as it does not absorb light with so long wavelengths.

We would like to mention the following general trend: in studies into the photocatalytic properties of Aurivillius phases (especially their composite photocatalysts), the researchers primarily intend to solve synthetic problems associated with the optimization of parameters to produce desired products and the development of new synthetic methods. Photocatalytic properties obtain far less attention, which has no good effect on the quality of data and their competent interpretation. The quantum efficiency, which is an important characteristic of the photocatalytic process, is determined only in few studies.[184, 247, 249] Usually, the authors merely compare the photocatalytic activities of the test sample and some reference sample, which is often synthesized in the same laboratory. Unfortunately, such a comparison fails to show the actual efficiency of a photocatalyst and its actual potential for use.

VIII. Conclusion

We have here surveyed the photocatalytic properties of three major classes of layered perovskite-like oxides, namely Ruddlesden–Popper, Dion–Jacobson and Aurivillius phases. Our analysis of the related literature focused on relationships between the physicochemical properties of layered oxides and their photocatalytic activities. The photocatalytic activity depends on obvious factors, such as the band gap energy, crystallinity and specific surface area, and also on the capability to intercalate substrate molecules into the interlayer space, which distinguishes layered oxides as a specific class of photocatalytic systems. A considerable enhancement of photocatalytic activity can be attained by the modifying methods specific for layered oxides, namely cation exchange (including protonation) and exfoliation. Composite photocatalysts based on layered perovskite-like oxides created by these methods, can have enhanced photocatalytic efficiencies and expanded spectral ranges of performance.

To conclude with, we would like to shortly dwell on some of the most important results.

Ruddlesden–Popper and Dion–Jacobson phases feature high activities in UV light-driven water splitting. A maximal quantum efficiency, equal to 5%, was achieved for the titanate $Rb_2La_2Ti_3O_{10}/NiO_x$ at the wavelength of 330 nm (a Ruddlesden–Popper phase)[91] and for tantalates $NaCa_2Ta_3O_{10}/NiO_x$ irradiated with the complete spectrum of a high-pressure mercury lamp (a Dion–Jacobson phase).[173] This value exceeds the quantum efficiency of $K_4Nb_6O_{17}$ at 330 nm (3.5%).[21] This high activity is due to the intercalation of water molecules into the interlayer space, which is typical for representatives of these classes of compounds.

The replacement of interlayer cations by protons results in a considerable (1–2 orders of magnitude) enhacement of the photocatalytic activity of $ACa_2Nb_3O_{10}$ niobates in the reaction of hydrogen evolution from aqueous methanol due to the ability of protonated species to intercalation.[65] The protonation reaction is also an important stage in the modifying of layered oxides *via* the intercalation of organic bases into the

interlayer space and subsequent ion exchange to produce composite photocatalysts.[27, 141, 142, 166]

The exfoliation of Dion–Jacobson phases as a result of intercalation of organic bases makes it possible to obtain dispersions of perovskite nanosheets, which serves to create composite photocatalysts having high specific surface areas.[97] In the case of $KCa_2Nb_3O_{10}$, this was the only modification strategy that succeeded to generate photocatalytic activity in UV light-driven water splitting.[159]

Aurivillius phases are active under the visible light in the photocatalytic degradation of organic compounds in aqueous solution (dyes and phenols) and in a vapour phase (benzene, toluene and acetaldehyde) and in the reduction of carbon dioxide to methane. Intercalation reactions are not typical of Aurivillius phases. An enhancement of photocatalytic activity of them is achieved by classic methods of increasing specific surface area, improving crystallinity, generating tailored particle morphology, doping, creating composites or sensitizing. Aurivillius phases are active in the reactions of hydrogen and oxygen evolution from water in the presence of sacrifical agents under visible light and thereby are candidate components for two-photon photocatalytic systems. For $PbBi_2Nb_2O_9$, for example, the quantum efficiency in the reaction of hydrogen evolution from aqueous methanol solution (15 vol.%) is 0.95% ($\lambda > 420$ nm);[184] the quantum efficiency increases to 1.92% and 6%, respectively, in going to the tungsten-doped compound $PbBi_2Nb_{1.85}W_{0.15}O_9$ (Ref. 247) and the composite photocatalyst $WO_3/W/PbBi_2Nb_{1.9}Ti_{0.1}O_9$.[249]

In the context of the opportunities to enhance the photocatalytic activity of perovskite-like layered oxides and expand their performance spectral range to the visible, apart from well-known strategies (doping, increasing specific surface area and loading cocatalysts), noticeable are methods that use the advantages of layered structure. These methods are exemplified by insertion of functional groups in between perovskite layers to perform as a cocatalyst, a sensitizer or a constituent of a two-photon photocatalytic system. In all cases, the result is a nanostructured composite material that has a high area offered for the interaction between the constituents and, in some cases, a developed surface, which is preferable compared to an ordinary composite photocatalyst. From the body of surveyed literature, we can infer that there are now two main routes that will be helpful to insert such particles between layers. One route is to carry out an ion-exchange (intercalation) process in order to embed, into the interlayer space, either the desired compound directly or its precursor, which will form cocatalyst species[90, 169] or sensitizer species upon subsequence irradiation.[27, 142, 176] The other route involves the exfoliation of the oxide followed by restacking in the presence of a required modifier.[159] The matrices suitable for intercalation are usually compounds that are capable of ion exchange and have the Ruddlesden–Popper or Dion–Jacobson structure. Aurivillius phases can perform as modifiers in these composites dueto their ability to absorb visible light and rich opportunities for their preparation in nanosized state.

We would like to mention that the above-described strategies of the design of nanostructured composite photocatalysts are also applicable to other classes of layered oxides, in particular to layered titanates,[252, 253] which are not perovskite-like compounds and so are beyond the scope of this survey.

In general, our standpoint is that the design and use of efficient photocatalysts for splitting water and degrading organic contaminants, in organic synthesis and carbon dioxide reduction has a great potential, and perovskite-like layered oxides obviously deserve attention of those engaged in the art.

Now we will dwell on two methodological aspects that seem us to be important for progress in the art. First, in order to succeed in the preparation and application of new photocatalysts, one needs to know more about chemical properties of layered perovskite-like oxides. Specifically, one needs a detailed understanding of the processes that occur inside the interlayer space of a layered oxide in water and in organic solvents depending on conditions (pH, temperature and solution composition). This understanding will provide a more meaningful way to select conditions for ion-exchange and intercalation processes in order to prepare new photocatalysts and optimize the parameters of photocatalytic processes themselves. Ion-exchange and intercalation reactions in layered perovskite-like oxides are now far grom being completely studied, which is sometimes responsible for an incorrect design of experiments and a misleading interpretation of their results.

Secondly, there is need for improving experimental methods and forming common approaches to photocatalytic studies. Most of the studies covered by this review focus on the synthesis and modifying of layered oxides, while their photocatalytic properties obtain far less attention. In particular, most researchers in the context of photocatalytic activity refer only to the observed rate of the model reaction, but not its quantum efficiency. Meanwhile, quantum efficiency is just the quantity that enables the comparison of photocatalyst activities under dissimilar conditions and thereby evaluate the significance of results of the study. Not knowing quantum efficiencies for most of the photocatalytic systems addressed by this survey, we met much difficulties in systematizing the very rich experimental data set. In this context, it would be expedient to embed some standards and rules into photocatalytic experimental practices to help a researcher who will follow them to characterize the system under study as fully as possible. Some steps in this direction have already been taken,[52] and we can only welcome this.

We hope that this survey will be useful for researchers engaged in the chemistry and functional properties of layered oxides and in the design and investigation of new materials for heterogeneous photocatalysis.

The authors are grateful to O I Silyukov and A A Burovikhina for fruitful discussion.

The preparation of this review was financially supported by the Russian Foundation for Basic Research (Project Nos 12-03-00761, 14-03-31968 and 15-03-05981).

References

1. I I Moiseev *Russ. Chem. Rev.* **82** 616 (2013)
2. Y Sang, H Liu, A Umar *ChemCatChem* **7** 559 (2015)
3. R M N Yerga, M C Alvarez-Galvan, F Vaquero, J Arenales, J L G Fierro, in *Renewable Hydrogen Technologies* (Eds L M Gandia, G Arzamendi, P M Dieguez) (Amsteram: Elsevier, 2013) p. 43
4. A Kudo, Y Miseki *Chem. Soc. Rev.* **38** 253 (2009)
5. S C Roy, O K Varghese, M Paulose, C A Grimes *ACS Nano* **4** 1259 (2010)
6. Y Izumi *Coord. Chem. Rev.* **257** 171 (2013)
7. A Banerjee, B D Yuhas, E A Margulies, Y Zhang, Y Shim, M R Wasielewski, M G Kanatzidis *J. Am. Chem. Soc.* **137** 2030 (2015)
8. A V Vorontsov *Russ. Chem. Rev.* **77** 909 (2008)
9. M R Hoffmann, S T Martin, W Choi, D W Bahnemann *Chem. Rev.* **95** 69 (1995)
10. A S Besov, A V Vorontsov, V N Parmon *Appl. Catal., B* **89** 602 (2009)
11. M N Chong, B Jin, C W K Chow, C Saint *Water Res.* **44** 2997 (2010)
12. A V Vorontsov, G B Barannik, O I Snegurenko, E N Savinov, V N Parmon *Kinet. Catal.* **38** 84 (1997) [*Kinet. Katal.* **38** 97 (1997)]
13. O Carp, C L Huisman, A Reller *Prog. Solid State Chem.* **32** 33 (2004)
14. I A Zvereva, L M Kalinkina, I A Rodionov, A M Sankovich, I V Kolesnik, E A Gudilin *Glas. Phys. Chem.* **38** 504 (2012) [*Fiz. Khim. Stekla* **38** 733 (2012)]
15. H De Lasa, B Serrano, M Salaices *Photocatalytic Reaction Engineering* (New York: Springer, 2005)
16. X Chen, S Shen, L Guo, S S Mao *Chem. Rev.* **110** 6503 (2010)
17. K Maeda *J. Photochem. Photobiol., C* **12** 237 (2011)
18. F E Osterloh *Chem. Mater.* **20** 35 (2008)
19. K Maeda, K Domen, in *Comprehensive Inorganic Chemistry II*. (Eds J Reedijk, K Poeppelmeier) (Amsterdam: Elsevier, 2013) p. 587
20. A Ismail, D W Bahnemann *Sol. Energy Mater. Sol. Cells* **128** 85 (2014)
21. A Kudo, A Tanaka, K Domen, K Maruya, K Aika, T Onishi *J. Catal.* **111** 67 (1988)
22. G Centi, S Perathoner *Microporous Mesoporous Mater.* **107** 3 (2008)
23. R E Schaak, T E Mallouk *Chem. Mater.* **14** 1455 (2002)
24. M A Bizeto, A L Shiguiharao, V R L Constantino *J. Mater. Chem.* **19** 2512 (2009)
25. Y Cao, L Jiang, H Guo, Q Zheng *J. Mol. Catal., A* **383 – 384** 209 (2014)
26. Y Liang, M Shao, W Cui, L Liu, J G McEvoy *J. Mol. Catal., A* **370** 87 (2013)
27. W Cui, Y Liu, L Liu, J Hu, Y Liang *Appl. Catal., A* **417 – 418** 111 (2012)
28. S E Braslavsky, A M Braun, A E Cassano, A V Emeline, M I Litter, L Palmisano, V N Parmon, N Serpone *Pure Appl. Chem.* **83** 931 (2011)
29. V N Parmon *Catal. Today* **39** 137 (1997)
30. B Ohtani *Phys. Chem. Chem. Phys.* **16** 1788 (2014)
31. O V Gerasimov, V N Parmon *Russ. Chem. Rev.* **61** 154 (1992)
32. U I Gaya *Heterogeneous Photocatalysis Using Inorganic Semiconductor Solids* (Dordrecht: Springer, 2014)
33. A Emeline, A Salinaro, V K Ryabchuk, N Serpone *Int. J. Photoenergy* **3** 1 (2001)
34. P M Wood *Biochem. J.* **253** 287 (1988)
35. H A Schwarz *J. Chem. Educ.* **58** 101 (1981)
36. K Zeng, D Zhang *Prog. Energy Combust. Sci.* **36** 307 (2010)
37. J Yang, D Wang, H Han, C Li *Acc. Chem. Res.* **46** 1900 (2013)
38. A V Vorontsov, E A Kozlova, A S Besov, D V Kozlov, S A Kiselev, A S Safatov *Kinet. Catal.* **51** 801 (2010) [*Kinet. Katal.* **51** 829 (2010)]
39. I A Rodionov, E V Mechtaeva, I A Zvereva *Russ. J. Gen. Chem.* **84** 611 (2014) [*Zh. Obshch. Khim.* **84** 529 (2014)]
40. K Teramura, K Maeda, T Saito, T Takata, N Saito, Y Inoue, K Domen *J. Phys. Chem. B* **109** 21915 (2005)
41. B Ohtani *J. Photochem. Photobiol., C* **11** 157 (2010)
42. K Maeda, A Xiong, T Yoshinaga, T Ikeda, N Sakamoto, T Hisatomi, M Takashima, D Lu, M Kanehara, T Setoyama, T Teranishi, K Domen *Angew. Chem., Int. Ed.* **49** 4096 (2010)
43. A Kudo, H Kato, S Nakagawa *J. Phys. Chem. B* **104** 571 (2000)
44. H Kato, A Kudo *J. Phys. Chem. B* **105** 4285 (2001)
45. V Ryabchuk *Int. J. Photoenergy* **6** 95 (2004)
46. E M Sabio, R L Chamousis, N D Browning, F E Osterloh *J. Phys. Chem. C* **116** 3161 (2012)
47. A N Bugrov, I A Rodionov, R Y Smyslov, O V Almjasheva, I A Zvereva *Int. J. Nanotechnol.* **13** 147 (2016)
48. H Jeong, T Kim, D Kim, K Kim *Int. J. Hydrogen Energy* **31** 1142 (2006)
49. V K Ivanov, V D Maksimov, A S Shaporev, A E Baranchikov, B P Churagulov, I A Zvereva, Y D Tret'yakov *Russ. J. Inorg. Chem.* **55** 150 (2010) [*Zh. Neorg. Khim.* **55** 154 (2010)]
50. A I Gavrilov, I A Rodionov, D Y Gavrilova, I A Zvereva, B R Churagulov, Y D Tretyakov *Dokl. Chem.* **444** 133 (2012) [*Dokl. Akad. Nauk* **444** 510 (2012)]
51. B Ohtani *Chem. Lett.* **37** 216 (2008)
52. J M Buriak, P V Kamat, K S Schanze *ACS Appl. Mater. Interfaces* **6** 11815 (2014)
53. A V Vorontsov, A V Arsentyev *Curr. Org. Chem.* **17** 2459 (2013)
54. M Cherevatskaya, B König *Russ. Chem. Rev.* **83** 183 (2014)
55. V P Ananikov, L L Khemchyan, Y V Ivanova, V I Bukhtiyarov, A M Sorokin, I P Prosvirin, S Z Vatsadze, A V Medved'ko, V N Nuriev, A D Dilman, V V Levin, I V Koptyug, K V Kovtunov, V V Zhivonitko, V A Likholobov, A V Romanenko, P A Simonov, V G Nenajdenko, O I Shmatova, V M Muzalevskiy, M S Nechaev, A F Asachenko, O S Morozov, P B Dzhevakov, S N Osipov, D V Vorobyeva, M A Topchiy, M A Zotova, S A Ponomarenko, O V Borshchev, Y N Luponosov, A A Rempel, A A Valeeva, A Y Stakheev, O V Turova, I S Mashkovsky, S V Sysolyatin, V V Malykhin, G A Bukhtiyarova, A O Terent'ev, I B Krylov *Russ. Chem. Rev.* **83** 885 (2014)
56. M A Fox, M A Fox, M T Dulay, M T Dulay *Chem. Rev.* **93** 341 (1993)
57. P R Gogate, A B Pandit *Adv. Environ. Res.* **8** 501 (2004)
58. J Sa *Fuel Production with Heterogeneous Catalysis* (Boca Raton, FL: CRC Press, 2015)

59. H Kisch, in *Advances in Photochemistry* (Eds D C Neckers, G von Bünau, W S Jenks) (New York; Wiley, 2001) p. 93
60. A Fujishima, K Honda *Nature (London)* **238** 37 (1972)
61. T Takata, A Tanaka, M Hara, J N Kondo, K Domen *Catal. Today* **44** 17 (1998)
62. S Ekambaram *J. Alloys Compd.* **448** 238 (2008)
63. M Matsuoka, M Kitano, M Takeuchi, K Tsujimaru, M Anpo, J M Thomas *Catal. Today* **122** 51 (2007)
64. I Zvereva, I Rodionov, in *Perovskite: Crystallography, Chemistry and Catalytic Performance* (Eds J Zhang, H Li) (New York: Nova Science Publishers, 2013) p. 181
65. K Domen, J Yoshimura, T Sekine, A Tanaka, T Onishi *Catal. Lett.* **4** 339 (1990)
66. T P Lyubina, D V Markovskaya, E A Kozlova, V N Parmon *Int. J. Hydrogen Energy* **38** 14172 (2013)
67. E A Kozlova, N S Kozhevnikova, S V Cherepanova, T P Lyubina, E Y Gerasimov, V V Kaichev, A V Vorontsov, S V Tsybulya, A A Rempel, V N Parmon *J. Photochem. Photobiol., A* **250** 103 (2012)
68. K Fujihara, T Ohno, M Matsumura *J. Chem. Soc., Faraday Trans.* **94** 3705 (1998)
69. K Sayama, K Mukasa, R Abe, Y Abe, H Arakawa *J. Photochem. Photobiol., A* **148** 71 (2002)
70. J Schneider, D W Bahnemann *J. Phys. Chem. Lett.* **4** 3479 (2013)
71. F Han, V S R Kambala, M Srinivasan, D Rajarathnam, R Naidu *Appl. Catal., A* **359** 25 (2009)
72. A A Sadovnikov, A E Baranchikov, Y V Zubavichus, O S Ivanova, V Y Murzin, V V Kozik, V K Ivanov *J. Photochem. Photobiol., A* **303**–**304** 36 (2015)
73. I K Konstantinou, T A Albanis *Appl. Catal., B* **49** 1 (2004)
74. A Houas, H Lachheb, M Ksibi, E Elaloui, C Guillard, J M Herrmann *Appl. Catal., B* **31** 145 (2001)
75. J Bandara, J A Mielczarski, J Kiwi *Langmuir* **15** 7680 (1999)
76. X Yan, T Ohno, K Nishijima, R Abe, B Ohtani *Chem. Phys. Lett.* **429** 606 (2006)
77. F Lichtenberg, A Herrnberger, K Wiedenmann *Prog. Solid State Chem.* **36** 253 (2008)
78. S N Ruddlesden, P Popper *Acta Crystallogr.* **10** 538 (1957)
79. S N Ruddlesden, P Popper *Acta Crystallogr.* **11** 54 (1958)
80. M Dion, M Ganne, L De Chimie, M Dion *Mater. Res. Bull.* **16** 1429 (1981)
81. A J Jacobson, J T Lewandowski, W Johnson *J. Less-Common Met.* **116** 137 (1986)
82. A J Jacobson, J W Johnson, J T Lewandowski *Mat. Res. Bull.* **22** 45 (1987)
83. B Aurivillius *Ark. Kemi* **1** 463 (1949)
84. G A Smolenskii, V A Isupov, A I Agranovskaya *Fiz. Tv. Tela* **1** 169 (1959)
85. J Gopalakrishnan, V Bhat *Inorg. Chem.* **26** 4299 (1987)
86. T Mitsuyama, A Tsutsumi, T Hata, K Ikeue, M Machida *Bull. Chem. Soc. Jpn.* **81** 401 (2008)
87. M Machida, K Miyazaki, S Matsushima, M Arai *J. Mater. Chem.* **13** 1433 (2003)
88. O Silyukov, M Chislov, A Burovikhina, T Utkina, I Zvereva *J. Therm. Anal. Cal.* **110** 187 (2012)
89. O I Silyukov, L D Abdulaeva, A A Burovikhina, I A Rodionov, I A Zvereva *J. Solid State Chem.* **226** 101 (2015)
90. A Kudo, K Sayama, A Tanaka, K Asakura, K Domen, K Maruya, T Onishi *J. Catal.* **120** 337 (1989)
91. T Takata, Y Furumi, K Shinohara, A Tanaka, M Hara, J N Kondo, K Domen *Chem. Mater.* **9** 1063 (1997)
92. M Hayward, in *Comprehensive Inorganic Chemistry II* (Eds J Reedijk, K Poeppelmeier) (Amsterdam: Elsevier, 2013) p. 417
93. R E Schaak, T E Mallouk *J. Solid State Chem.* **161** 225 (2001)
94. J Gopalakrishnan, T Sivakumar, K Ramesha, V Thangadurai, G N Subbanna *J. Am. Chem. Soc.* **122** 6237 (2000)
95. V Nicolosi, M Chhowalla, M G Kanatzidis, M S Strano, J N Coleman *Science* **340** 1226419 (2013)
96. Y Ebina, T Sasaki, M Watanabe *Solid State Ionics* **151** 177 (2002)
97. Y Ebina, T Sasaki, M Harada, M Watanabe *Chem. Mater.* **14** 4390 (2002)
98. L D Abdulaeva, O I Silyukov, Y V Petrov, I A Zvereva *J. Nanomater.* 1 (2013)
99. M Fang, C H Kim, G B Saupe, H-N Kim, C C Waraksa, T Miwa, A Fujishima, T E Mallouk *Chem. Mater.* **11** 1526 (1999)
100. S W Keller, H Kim, T E Mallouk *J. Am. Chem. Soc.* **116** 8817 (1994)
101. H Zhou, E M Sabio, T K Townsend, T Fan, D Zhang, F E Osterloh *Chem. Mater.* **22** 3362 (2010)
102. K Domen, A Kudo, A Shinozaki, A Tanaka, K Maruya, T Onishi *J. Chem. Soc., Chem. Commun.* 356 (1986)
103. K Nassau, J W Shiever, L Bernstein *J. Electrochem. Soc. Solid State Sci.* **116** 348 (1969)
104. M Gasperin, M T Le Bihan *J. Solid State Chem.* **33** 83 (1980)
105. M Gasperin, M T Le Bihan *J. Solid State Chem.* **43** 346 (1982)
106. N Kinomura, N Kumada, F Muto *J. Chem. Soc., Dalton Trans.* 2349 (1985)
107. K Sayama, A Tanaka, K Domen, K Maruya, T Onishi *J. Catal.* **124** 541 (1990)
108. K Sayama, A Tanaka, K Domen, K Maruya, T Onishi *J. Phys. Chem.* **95** 1345 (1991)
109. K Sayama, K Yase, H Arakawa, K Asakura, A Tanaka, K Domen, T Onishi *J. Photochem. Photobiol., A* **114** 125 (1998)
110. H Arakawa, K Sayama *Catal. Surv. Jpn.* **4** 75 (2000)
111. K Domen, A Kudo, M Shibata, A Tanaka, K Maruya, T Onishi *J. Chem. Soc., Chem. Commun.* 1706 (1986)
112. K Domen, Y Ebina, S Ikeda, A Tanaka, J Kondo, K Maruya *Catal. Today* **28** 167 (1996)
113. M C Sarahan, E C Carroll, A Mark, D S Larsen, N D Browning, F E Osterloh *J. Solid State Chem.* **181** 1678 (2008)
114. K Maeda, M Eguchi, W J Youngblood, T E Mallouk *Chem. Mater.* **20** 6770 (2008)
115. K Toda, J Watanabe, M Sato *Mater. Res. Bull.* **31** 1427 (1996)
116. S Uma, A R Raju, J Gopalakrishnan *J. Mater. Chem.* **3** 709 (1993)

117. T Takata, K Shinohara, A Tanaka, M Hara, J N Kondo, K Domen *J. Photochem. Photobiol., A* **106** 45 (1997)
118. S Byeon, H Nam *Chem. Mater.* **12** 1771 (2000)
119. I A Rodionov, O I Silyukov, T D Utkina, M V Chislov, Y P Sokolova, I A Zvereva *Russ. J. Gen. Chem.* **82** 1191 (2012) [*Zh. Obshch. Khim.* **82** 1064 (2012)]
120. Y Huang, J Wu, Y Wei, S Hao, M Huang, J Lin *Scr. Mater.* **57** 437 (2007)
121. Y Yang, Q Chen, Z Yin, J Li *Chin. J. Inorg. Chem.* **23** 771 (2007)
122. Y Yang, Q Chen, J Li *Chin. J. Catal.* **30** 147 (2009)
123. Y Yang, Q Chen, J Li, Z Yin *Chin. J. Inorg. Chem.* **25** 256 (2009)
124. Y Yang, Q Chen, Z Yin, J Li *Appl. Surf. Sci.* **255** 8419 (2009)
125. Y Yang, Q Chen, Z Yin, J Li *J. Alloys Compd.* **48** 364 (2009)
126. W Chen, X-F Dong, Z-S Chen, S-Z Chen, W-M Lin *Acta Phys.-Chim. Sin.* **25** 1107 (2009)
127. Y Huang, Y Wei, S Cheng, L Fan, Y Li, J Lin, J Wu *Sol. Energy Mater. Sol. Cells* **94** 761 (2010)
128. L Liu, W Cui, Y Liang, F Qiu *Acta Chim. Sin.* **68** 211 (2010)
129. B Wang, C Li, D Hirabayashi, K Suzuki *Int. J. Hydrogen Energy* **35** 3306 (2010)
130. V Kumar, Govind, S Uma *J. Hazard. Mater.* **189** 502 (2011)
131. S Ikeda, M Hara, J N Kondo, K Domen *Chem. Mater.* **10** 72 (1998)
132. S Ikeda, M Hara, J N Kondo, K Domen *J. Mater. Res.* **13** 852 (1998)
133. L Zhang, W Zhang, J Zhu, L Lu, X Yang, X Wang *J. Solid State Chem.* **178** 761 (2005)
134. Y Yang, G Qiu, Q Chen, Q Feng, Z Yin *Trans. Nonferrous Met. Soc. China* **17** 836 (2007)
135. Y Huang, J Wu, Y Wei, J Lin, M Huang *J. Alloys Compd.* **456** 364 (2008)
136. W Cui, Y Qi, J Hu, Y Liang *Adv. Mater. Res.* **415 – 417** 1992 (2012)
137. I A Rodionov, O I Silyukov, I A Zvereva *Russ. J. Gen. Chem.* **82** 635 (2012) [*Zh. Obshch. Khim.* **82** 548 (2012)]
138. C Thaminimulla, T Takata, M Hara, J Kondo, K Domen *J. Catal.* **196** 362 (2000)
139. Y-W Tai, J-S Chen, C-C Yang, B-Z Wan *Catal. Today* **97** 95 (2004)
140. W Cui, L Liu, L Feng, C Xu, Z Li, S Lü, F Qiu *Sci. Chin., Ser. B* **49** 162 (2006)
141. Y Huang, J Wu, T Li, S Hao, J Lin *J. Porous Mater.* **13** 55 (2006)
142. J Wu, Y Huang, T Li, J Lin, M Huang, Y Wei *Scr. Mater.* **54** 1357 (2006)
143. L Zhang, W Zhang, L Lu, X Yang, X Wang *J. Mater. Sci.* **41** 3917 (2006)
144. W Cui, Y Qi, J Hu, L Liu, Y Liang *Acta Chim. Sin.* **70** 691 (2012)
145. W-Q Cui, Y-L Qi, Y-F Liu, L Liu, L-H Fan, J-S Hu, Y-H Liang *J. Inorg. Mater.* **27** 1145 (2012)
146. Y-H Liang, W-Q Cui, L Liu, Y-L Qi *J. Funct. Mater.* **44** 974 (2013)
147. W Cui, Y Qi, L Liu, D Rana, J Hu, Y Liang *Prog. Nat. Sci. Mater. Int.* **22** 120 (2012)
148. W Cui, L Liu, S Ma, Y Liang, Z Zhang *Catal. Today* **207** 44 (2013)
149. R E Schaak, T E Mallouk *Chem. Mater.* **12** 3427 (2000)
150. S Ida, C Ogata, M Eguchi, W J Youngblood, T E Mallouk, Y Matsumoto *J. Am. Chem. Soc.* **130** 7052 (2008)
151. C Ogata, S Ida, Y Matsumoto *IOP Conf. Ser. Mater. Sci. Eng.* **1** 012004 (2009)
152. K Toda, T Teranishi, Z-G Ye, M Sato, Y Hinatsu *Mater. Res. Bull.* **34** 971 (1999)
153. K Toda, T Honma, Z-G Ye, M Sato *J. Alloys Compd.* **249** 256 (1997)
154. K Toda, M Sato *J. Mater. Chem.* **6** 1067 (1996)
155. J Gopalakrishnan, V Bhat, B Raveau *Mater. Res. Bull.* **22** 413 (1987)
156. C H Mahler, B L Cushing, J N Lalena, J B Wiley *Mater. Res. Bull.* **33** 1581 (1998)
157. A J Jacobson, J T Lewandowski, J W Johnson *Mater. Res. Bull.* **25** 679 (1990)
158. J Gopalakrishnan, S Uma, V Bhat *Chem. Mater.* **5** 132 (1993)
159. Y Ebina, N Sakai, T Sasaki *J. Phys. Chem. B* **109** 17212 (2005)
160. O C Compton, E C Carroll, J Y Kim, D S Larsen, F E Osterloh *J. Phys. Chem. C* **111** 14589 (2007)
161. O C Compton, C H Mullet, S Chiang, F E Osterloh *J. Phys. Chem. C* **112** 6202 (2008)
162. Y Chen, X Zhao, H Ma, S Ma, G Huang, Y Makita, X Bai, X Yang *J. Solid State Chem.* **181** 1684 (2008)
163. H Hata, Y Kobayashi, V Bojan, W J Youngblood, T E Mallouk *Nano Lett.* **8** 794 (2008)
164. Y Chen, S Zhou, X Yang, Y Ou-Yang *J. Solid State Chem.* **183** 823 (2010)
165. A A Burovikhina, I A Rodionov, M V Chislov, D A Porotnikov, I A Zvereva *Int. J. Nanotechnol.* **13** 158 (2016)
166. K Domen, Y Ebina, J Kondo *Res. Chem. Intermed.* **20** 895 (1994)
167. K Maeda, T E Mallouk *J. Mater. Chem.* **19** 4813 (2009)
168. M A Subramanian, J Gopalakrishnan, A W Sleight *Mater. Res. Bull.* **23** 837 (1988)
169. J Yoshimura, Y Ebina, J Kondo, K Domen *J. Phys. Chem.* **97** 1970 (1993)
170. Y Hu, J Shi, L Guo *Appl. Catal., A* **468** 403 (2013)
171. Y Huang, Y Xie, L Fan, Y Li, Y Wei, J Lin, J Wu *Int. J. Hydrogen Energy* **33** 6432 (2008)
172. Y Hu, P Guo, L Guo *Int. J. Hydrogen Energy* **37** 1007 (2012)
173. M Machida, T Mitsuyama, K Ikeue *J. Phys. Chem. B* **109** 7801 (2005)
174. T Mitsuyama, A Tsutsumi, S Sato, K Ikeue, M Machida *J. Solid State Chem.* **181** 1419 (2008)
175. Y Huang, Y Li, Y Wei, M Huang, J Wu *Sol. Energy Mater. Sol. Cells* **95** 1019 (2011)
176. Y Wei, X Zhang, J Xu, J Wang, Y Huang, L Fan, J Wu *Appl. Catal., B* **147** 920 (2014)
177. S Ida, Y Okamoto, M Matsuka, H Hagiwara, T Ishihara *J. Am. Chem. Soc.* **134** 15773 (2012)
178. M Machida, J Yabunaka, T Kijima *Chem. Commun.* 1939 (1999)
179. M Machida, J Yabunaka, T Kijima *Chem. Mater.* **12** 812 (2000)
180. M Machida, J Yabunaka, T Kijima, S Matsushima *Int. J. Inorg. Mater.* **3** 545 (2001)
181. A A Burovikhina, M V Chislov, I A Rodionov, D A Porotnikov, I A Zvereva *Russ. J. Gen. Chem.* **84** 1893 (2014) [*Zh. Obshch. Khim.* **84** 1612 (2014)]

182. K S Knight *Mineral. Mag.* **56** 399 (1992)
183. R W G Wyckoff *The Structure of Crystals* (New York: Interscience, 1951)
184. H G Kim, D W Hwang, J S Lee *J. Am. Chem. Soc.* **126** 8912 (2004)
185. R G Teller, J F Brazdil, R K Grasselli, J D Jorgensen *Acta Crystallogr., Sect. C* **40** 2001 (1984)
186. W Chen, X Chen, Y Yang, J Yuan, W Shangguan *Int. J. Hydrogen Energy* **9** 2 (2014)
187. W Chen, C Li, H Gao, J Yuan, W Shangguan, J Su, Y Sun *Int. J. Hydrogen Energy* **37** 12846 (2012)
188. H G Kim, O S Becker, J S Jang, S M Ji, P H Borse, J S Lee *J. Solid State Chem.* **179** 1214 (2006)
189. L Zhou, W Wang, L Zhang *J. Mol. Catal. A: Chem.* **268** 195 (2007)
190. Y Li, G Chen, H Zhang, Z Li, J Sun *J. Solid State Chem.* **181** 2653 (2008)
191. Y Li, G Chen, H Zhang, Z Lv *Int. J. Hydrogen Energy* **35** 2652 (2010)
192. D Wang, K Tang, Z Liang, H Zheng *J. Solid State Chem.* **183** 361 (2010)
193. J S Lee *Catal. Surv.Asia* **9** 217 (2006)
194. C Belver, C Adán, M Fernández-García *Catal. Today* **143** 274 (2009)
195. A Martínez-de la Cruz, S Obregón Alfaro, E López Cuéllar, U Ortiz Méndez *Catal. Today* **129** 194 (2007)
196. H Xie, D Shen, X Wang, G Shen *Mater. Chem. Phys.* **110** 332 (2008)
197. J Bi, L Wu, J Li, Z Li, X Wang, X Fu *Acta Mater.* **55** 4699 (2007)
198. Y Zheng, F Duan, J Wu, L Liu, M Chen, Y Xie *J. Mol. Catal. A: Chem.* **303** 9 (2009)
199. C Xu, X Wei, Z Ren, Y Wang, G Xu, G Shen, G Han *Mater. Lett.* **63** 2194 (2009)
200. L Wu, J Bi, Z Li, X Wang, X Fu *Catal. Today* **131** 15 (2008)
201. S Zhang, C Zhang, Y Man, Y Zhu *J. Solid State Chem.* **179** 62 (2006)
202. L Zhang, K-H Wong, Z Chen, J C Yu, J Zhao, C Hu, C-Y Chan, P-K Wong *Appl. Catal., A* **363** 221 (2009)
203. P Dumrongrojthanath, T Thongtem, A Phuruangrat, S Thongtem *Superlatt. Microstruct.* **64** 196 (2013)
204. W F Yao, H Wang, X H Xu, S X Shang, Y Hou, Y Zhang, M Wang *Mater. Lett.* **57** 1899 (2003)
205. H Zhang, M Lm, S Liu, L Wang, Z Xiu, Y Zhou, Z Qiu, A Zhang, Q Ma *Mater. Chem. Phys.* **114** 716 (2009)
206. W Yao *Appl. Catal., A* **251** 235 (2003)
207. J Bi, L Wu, Z Li, X Wang, X Fu *Mater. Lett.* **62** 155 (2008)
208. V L Blair, E J Nichols, J Liu, S T Misture *Appl. Surf. Sci.* **268** 410 (2013)
209. Y Liu, H Lv, J Hu, Z Li *Mater. Lett.* **139** 401 (2015)
210. X Wang, L Chang, J Wang, N Song, H Liu, X Wan *Appl. Surf. Sci.* **270** 685 (2013)
211. X Wang, P Tian, Y Lin, L Li *J. Alloys Compd.* **620** 228 (2015)
212. X Lin, Q Guan, T-T Liu, Y Zhang, C-J Zou *Acta Phys.-Chim. Sin.* **29** 411(2013)
213. E Luévano-Hipólito, A Martínez-de la Cruz, E López Cuéllar *J. Taiwan Inst. Chem. Eng.* **45** 2749 (2014)
214. X Lin, Y Gong, Y Zhang, Y Yan, Q Guan *Chin. J. Chem. Phys.* **27** 209 (2014)
215. A Phuruangrat, A Maneechote, P Dumrongrojthanath, N Ekthammathat, S Thongtem, T Thongtem *Superlatt. Microstruct.* **78** 106 (2015)
216. D-K Ma, S-M Zhou, X Hu, Q-R Jiang, S -M Huang *Mater. Chem. Phys.* **140** 11 (2013)
217. Y Zhou, Z Tian, Z Zhao, Q Liu, J Kou, X Chen, J Gao, S Yan, Z Zou *ACS Appl. Mater. Interfaces* **3** 3594 (2011)
218. L Wang, W Ma, Y Fang, Y Zhang, M Jia, R Li, Y Huang *Proc. Environ. Sci.* **18** 547 (2013)
219. A E Nogueira, E Longo, E R Leite, E R Camargo *J. Colloid Interface Sci.* **415** 89 (2014)
220. Y Miao, G Pan, Y Huo, H Li *Dyes Pigm.* **99** 382 (2013)
221. Z Zhang, W Wang, W Yin, M Shang, L Wang, S Sun *Appl. Catal., B* **101** 68 (2010)
222. Z Zhang, W Wang, E Gao, M Shang, J Xu *J. Hazard. Mater.* **196** 255 (2011)
223. Q Wu, Y Cui, L Yang, G Zhang, D Gao *Sep. Purif. Technol.* **142** 168 (2015)
224. G Fu, G Xu, S Chen, L Lei, M Zhang *Catal. Commun.* **40** 120 (2013)
225. Z Zhang, W Wang, D Jiang, J Xu *Catal. Commun.* **55** 15 (2014)
226. M Zhang, Y Liu, L Li, H Gao, X Zhang *Catal. Commun.* **58** 122 (2015)
227. R M Mohamed, F M Ibrahim *J. Ind. Eng. Chem.* **22** 28 (2015)
228. Y Chen, X Cao, J Kuang, Z Chen, J Chen, B Lin *Catal. Commun.* **12** 247 (2010)
229. Z Sun, X Li, S Guo, H Wang, Z Wu *J. Colloid Interface Sci.* **412** 31 (2013)
230. M Hojamberdiev, K Katsumata, K Morita, S A Bilmes, N Matsushita, K Okada *Appl. Catal., A* **457** 12 (2013)
231. B V Kumar, M D Prasad, M Vithal *Mater. Lett.* **152** 200 (2015)
232. S Sriwichai, H Ranwongsa, K Wetchakun, S Phanichphant, N Wetchakun *Superlatt. Microstruct.* **76** 362 (2014)
233. A A Alemi, R Kashfi, B Shabani *J. Mol. Catal., A* **392** 290 (2014)
234. H Yu, Z Zhu, J Zhou, J Wang, J Li, Y Zhang *Appl. Surf. Sci.* **265** 424 (2013)
235. A Phuruangrat, S Putdum, P Dumrongrojthanath, N Ekthammathat, S Thongtem, T Thongtem *Mater. Sci. Semicond. Proc.* **34** 175 (2015)
236. B Yuan, C Wang, Y Qi, X Song, K Mu, P Guo, L Meng, H Xi *Colloids Surf., A* **425** 99 (2013)
237. R M Mohamed, E S Aazam *Mater. Res. Bull.* **48** 3572 (2013)
238. P Ju, P Wang, B Li, H Fan, S Ai, D Zhang, Y Wang *Chem. Eng. J.* **236** 430 (2014)
239. Z Zhang, W Wang, D Jiang, J Xu *Appl. Surf. Sci.* **292** 948 (2014)
240. Y Liu, M Zhang, L Li, X Zhang *Appl. Catal., B* **160** – **161** 757 (2014)
241. B Chen, Y Deng, H Tong, J Ma *Superlatt. Microstruct.* **69** 194 (2014)
242. X Hou, Y Tian, X Zhang, S Dou, L Pan, W Wang, Y Li, J Zhao *J. Alloys Compd.* **638** 214 (2015)
243. F Zhou, R Shi, Y Zhu *J. Mol. Catal., A,* **340** 77 (2011)
244. L Ge, C Han, J Liu *Appl. Catal., B* **108** – **109** 100 (2011)
245. H Wang, J Lu, F Wang, W Wei, Y Chang, S Dong *Ceram. Int.* **40** 9077 (2014)
246. W Chen, G-R Duan, T-Y Liu, S-M Chen, X-H Liu *Mater. Sci. Semicond. Proc.* **35** 45 (2015)
247. H G Kim, P H Borse, J S Jang, E D Jeong, J S Lee *Mater. Lett.* **62** 1427 (2008)

248. H Zhang, G Chen, X Li *Solid State Ionics* **180** 1599 (2009)
249. H G Kim, E D Jeong, P H Borse, S Jeon, K Yong, J S Lee, W Li, S H Oh *Appl. Phys. Lett.* **89** 064103 (2006)
250. H G Kim, P H Borse, W Choi, J S Lee *Angew. Chem., Int. Ed.* **117** 4661 (2005)
251. G Dong, Y Zhang, Q Pan, J Qiu *J. Photochem. Photobiol., C* **20** 33 (2014)
252. Y Zhang, H Liu, G Zhang, L He, P Liu, B Lin *Mater. Res. Bull.* **60** 510 (2014)
253. B Li, B Z Lin, O Zhang, L M Fu, H Liu, Y L Chen, B F Gao *J. Colloid Interface Sci.* **386** 1 (2012)